Electronic Supplementary Material (ESI) for ChemComm.
This journal is © The Royal Society of Chemistry 2022

Electronic Supplementary Information:

Long-Lived Charge Separated State and Thermally Activated Delayed Fluorescence in Anthraquinone-Phenoxazine Electron Donor-Acceptor Dyads

Xiaoyu Zhao,[a,b] and Jianzhang Zhao*[a,b]

[a] State Key Laboratory of Chemistry and Utilization of Carbon Based Energy Resources; College of Chemistry, Xinjiang University, Urumqi 830017, P. R. China.

[b] State Key Laboratory of Fine Chemicals, School of Chemical Engineering, Dalian University of Technology, Dalian 116024, P. R. China. *E-mail: zhaojzh@dlut.edu.cn

Index

1. Experimental Section

1.1 General Information. All the chemicals used in synthesis are analytically pure and were used as received. Solvents were dried prior to use. The molecular structures were fully verified with nuclear magnetic resonance (NMR), and high-resolution mass spectrometry (HRMS). NMR spectra were recorded on the Bruker Avance spectrometers (400 / 500 MHz). ^{1}H and ^{13}C chemical shifts are reported in parts per million (ppm) relative to tetramethylsilane (TMS), with the residual solvent peak used as an internal reference. UV–vis absorption spectra were measured on a Shimadzu UV-2550 UV–vis spectrophotometer (Shimadzu Ltd., Japan). Fluorescence spectra were recorded with FS5 spectrofluorometer (Edinburgh Instrument Ltd., U.K.). The fluorescence lifetimes were recorded on a OB920 luminescence lifetime spectrometer (Edinburgh Instrument Ltd., U.K.) equipped with 340 nm EPL picosecond pulsed laser for excitation, and the decay of the fluorescence were monitored with the time-correlated single photon counting (TCSPC) technique. The absolute fluorescence quantum yields were measured with a C13534 UV-NIR absolute photoluminescence quantum yield spectrometer, equipped with an optical integration sphere (Hamamatsu Photonics Ltd., Japan).

1.2 Cyclic Voltammetry. Cyclic voltammetry curves were recorded by a CHI610D electrochemical workstation (CHI instruments, Inc., Shanghai, China) at scan rate of 100 mV s^{-1}. Electrochemical measurements were performed at room temperature (RT) using 0.1 M tetrabutylammonium hexafluorophosphate ($Bu_4N[PF_6]$) as supporting electrolyte, a glassy carbon electrode as working electrode, and platinum electrode as counter electrode. The reference electrode was $Ag/AgNO_3$ (0.1 M in acetonitrile), and dichloromethane was used as the solvent. Ferrocene was added as the internal references. The measurement was performed under N_2 atmosphere.

1.3 Nanosecond Transient Absorption Spectroscopy. The nanosecond transient absorption (ns-TA) spectra were studied on LP920 laser flash-photolysis spectrometer (Edinburgh Instruments Ltd, U.K.), and the signal was digitized with a Tektronix TDS 3012B

oscilloscope. The data (kinetic decay traces and spectra) were analyzed with the L900 software. All samples for the measurements were deaerated with N_2 for about 15 min before measurement, and the samples was sealed during the measurement.

1.4 Density Functional Theory Calculations. The geometries of the dyads were optimized using density functional theory (DFT) with CAM-B3LYP functional and 6-31G (d) basis set. There are no imaginary frequencies for all optimized structures. The excitation energy and the energy gaps between ground state (S_0) and the triplet excited states (T_n) of the compounds were approximated at time-dependent density functional theory (TDDFT) tuned-CAM-B3LYP/6-31G (d) level with PCM model (solvent, cyclohexane and acetonitrile). The optimal ω value for the compounds was performed with optDFTw program v1.0[1] (the default range-separation parameter ω of 0.33 $bohr^{-1}$), the geometry of the compounds was re-optimized using the optimal ω value.[2] All these calculations were performed with Gaussian 16 Rev B01 program package.[3]

2. Synthesis of the Compounds

Scheme S1. Synthesis of the Compounds [a]

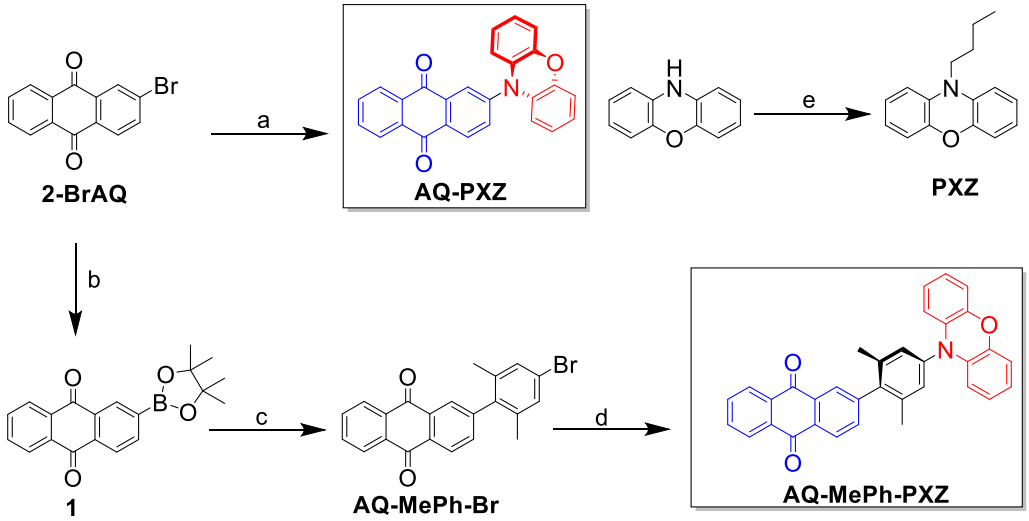

[a]Key: (a) Phenoxazine, $Pd_2(dba)_3$, tri-*tert*-butylphosphine, *t*-BuONa, dry toluene, N_2, stirred at reflux 24 h, yield: 77%; (b) Bis(pinacolate)diboron, $PdCl_2(dppf)\cdot CH_2Cl_2$, KOAc, dry 1,4-dioxane, stirred at reflux 24 h, yield: 68%; (c) 5-Bromo-2-iodo-1,3-dimethylbenzene, K_2CO_3, $Pd(PPh_3)_4$, toluene/ethanol/water = 4/2/1 (v/v/v), stirred at reflux 8 h, yield: 64%; (d) similar to step (a), yield: 84%; (e) *n*-C_4H_9Br, dry dimethylformamide, KOH, N_2, stirred at RT for 12 h, yield: 70%.

2.1 Synthesis of PXZ. The synthesis of **PXZ** was referred to the literature.[4] The crude product was purified by column chromatography (silica gel, PE/DCM = 10/1, v/v) to give **PXZ** as colorless oil (300 mg, yield: 77%). ^{1}H NMR (400 MHz, $CDCl_3$): δ = 6.79–6.45 (m, 8H), 3.46 (s, 2H), 1.67–1.59 (m, 2H), 1.47–1.38 (m, 2H), 1.04–0.98 (t, 3H, J = 7.3 Hz). HRMS (APCI, *m/z*) calcd for $C_{16}H_{18}NO$ $[M+H]^+$, 240.1388, found 240.1369.

2.2 Synthesis of Compound 1. 2-Bromoanthraquinone (1.0 g, 3.5 mmol), bis(pinacolate)diboron (1.1 g, 4.2 mmol) and KOAc (1.0 g, 10 mmol) were added to dry 1,4-dioxane (30 mL). The suspension was bubbled with nitrogen for 30 min and $PdCl_2(dppf)\bullet CH_2Cl_2$ (dppf = 1,1′-bis(diphenylphosphino)ferrocene) (140 mg, 0.2 mmol) was added. Kept in darkness, the reaction mixture was stirred at 80 °C for 12 h under nitrogen atmosphere. After completion of the reaction, the reaction mixture was cooled to RT. Then

saturated aqueous NH_4Cl solution (30 mL) was added and the mixture was extracted with ethyl acetate. The organic layer was dried by anhydrous Na_2SO_4 and the solvent was evaporated under reduced pressure. The crude product was purified by column chromatography (silica gel, PE/DCM = 2/1, v/v) to obtain a yellow solid (795 mg, yield: 68%). ^1H NMR ($CDCl_3$, 400 MHz) δ = 8.76 (s, 1 H), 8.35–8.30 (m, 3 H), 8.21 (d, 1 H, J = 7.7 Hz), 7.82–7.80 (m, 2 H), 1.39 (s, 12 H). HRMS (APCI, *m/z*) calcd for $C_{20}H_{20}BO_4^+$ $[M+H]^+$, 335.1454, found 335.1434.

2.3 Synthesis of AQ-MePh-Br. Compound 1 (334 mg, 1.0 mmol), 5-bromo-2-iodo-1,3-dimethylbenzene (372 mg, 1.2 mmol) and potassium carbonate (414 mg, 3.0 mmol) were dissolved in toluene/ethanol/water (4/2/1, v/v/v) in a 25 ml double neck flask. The suspension was bubbled with nitrogen for 30 min and $Pd(PPh_3)_4$ (85 mg, 0.08 mmol) was added. Kept in darkness, the reaction mixture was refluxed at 90 °C for 8 h under nitrogen atmosphere. After completed reaction, the mixture was extracted with dichloromethane (3 × 20 mL), and dried over anhydrous Na_2SO_4, and the solvent was evaporated under reduced pressure. The crude product was purified by column chromatography (silica gel, PE/DCM = 2/1, v/v) to give a purple solid (250 mg, yield: 64%). M.p.: 222.5–223.6 °C. ^1H NMR (400 MHz, $CDCl_3$): δ = 8.40 (d, 1 H, J = 7.9 Hz), 8.37–8.32 (m, 2 H), 8.10 (s, 1 H), 7.84–7.82 (m, 2 H), 7.57 (d, 1 H, J = 7.9 Hz), 7.31 (s, 2 H), 2.02 (s, 6 H). ^{13}C NMR (126 MHz, $CDCl_3$): δ = 183.12, 182.90, 146.65, 138.82, 137.69, 134.96, 134.24, 134.18, 133.86, 133.63, 132.45, 130.47, 127.83, 127.30, 121.73, 20.60. HRMS (APCI, *m/z*) calcd for $C_{22}H_{16}BrO_2^+$ $[M+H]^+$, 391.0333, found 391.0308.

2.4 Synthesis of AQ-PXZ. Under N_2 atmosphere, phenoxazine (275 mg, 1.5 mmol), 2–bromoanthraquinone (287 mg, 1.0 mmol), $Pd_2(dba)_3$ (3% mol, 27 mg), tri-*tert*-butylphosphine (6% mol, 12 mg) and sodium *tert*-butoxide (3 eq., 288 mg) were mixed in dry toluene (5 mL). The mixture was refluxed for 10 h at 120 °C. After the reaction, the mixture was extracted with dichloromethane (3 × 20 mL), and dried over anhydrous Na_2SO_4, and the solvent was evaporated under reduced pressure. The crude product was purified by column chromatography (silica gel, PE/DCM = 2/1, v/v) to give a purple solid (300 mg, yield: 77%). M.p.: > 250 °C. ^1H NMR (400 MHz, $CDCl_3$): δ = 8.53 (d, 1H, J = 8.2 Hz), 8.36–8.34 (m, 3H), 7.86–

7.80 (m, 3H), 6.79–6.71 (m, 4H), 6.65–6.62 (m, 2H), 6.05 (dd, 2H, *J* = 8.0, 1.4 Hz). ^{13}C NMR (126 MHz, $CDCl_3$): δ = 182.23, 145.41, 144.44, 136.30, 136.18, 134.45, 134.35, 133.52, 133.49, 133.21, 132.73, 130.43, 129.24, 127.46, 127.42, 123.39, 122.47. HRMS (ESI, *m*/*z*) calcd for $C_{26}H_{16}NO_3^+$ $[M+H]^+$, 390.1130, found 390.1114.

2.5 Synthesis of AQ-MePh-PXZ. The synthesis of **AQ-MePh-PXZ** was similar to **AQ-PXZ**. The crude product was purified by column chromatography (silica gel, PE/DCM = 2/1, v/v) to give a purple solid (108 mg, yield: 84%). M.p.: > 250 °C. ^{1}H NMR (400 MHz, $CDCl_3$): δ = 8.45 (d, 1 H, *J* = 7.9 Hz), 8.38–8.35 (m, 2 H), 8.20 (d, 1 H, *J* = 7.9 Hz), 7.84–7.82 (m, 2 H), 7.70 (d, 1 H, *J* = 7.9 Hz), 7.13 (s, 2 H), 6.71–6.63 (m, 5 H), 6.05 (s, 2 H), 2.09 (s, 6 H). ^{13}C NMR (126 MHz, $CDCl_3$): δ = 183.18, 182.93, 146.97, 144.01, 140.11, 138.70, 138.49, 135.02, 134.41, 134.27, 134.18, 133.90, 133.67, 133.65, 132.47, 129.55, 127.97, 127.86, 127.33, 127.32, 123.26, 121.30, 115.43, 113.40, 20.91. HRMS (APCI, m/z) calcd for $C_{34}H_{24}NO_3^+$ $[M+H]^+$, 494.1756, found 494.1731.

3. Molecular Structure Characterization Data

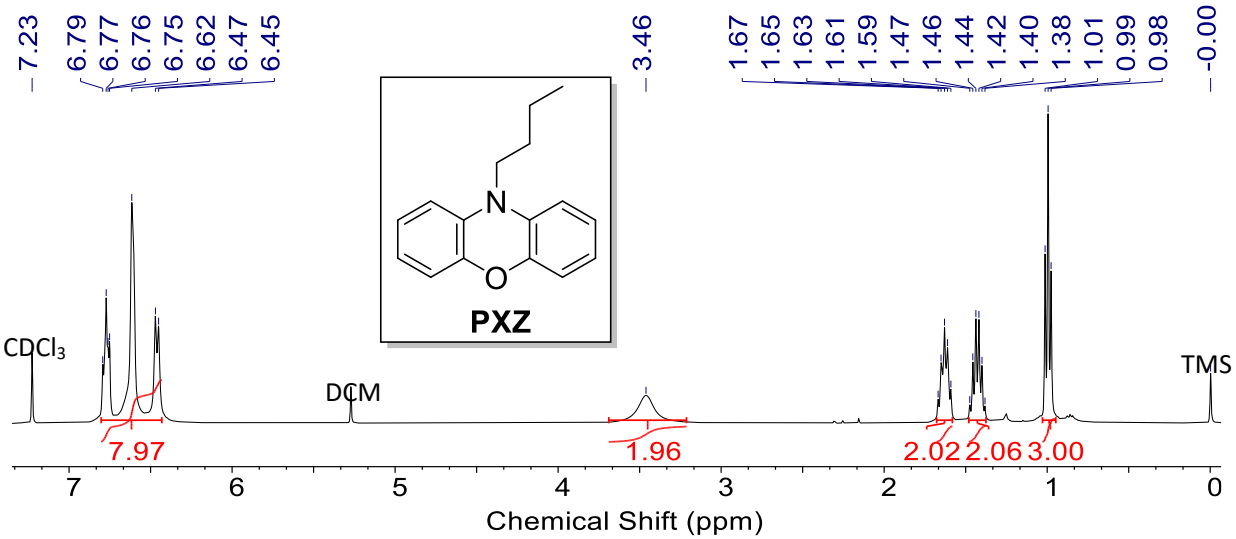

Fig. S1 ^{1}H NMR spectrum of **PXZ** (400 MHz, $CDCl_3$).

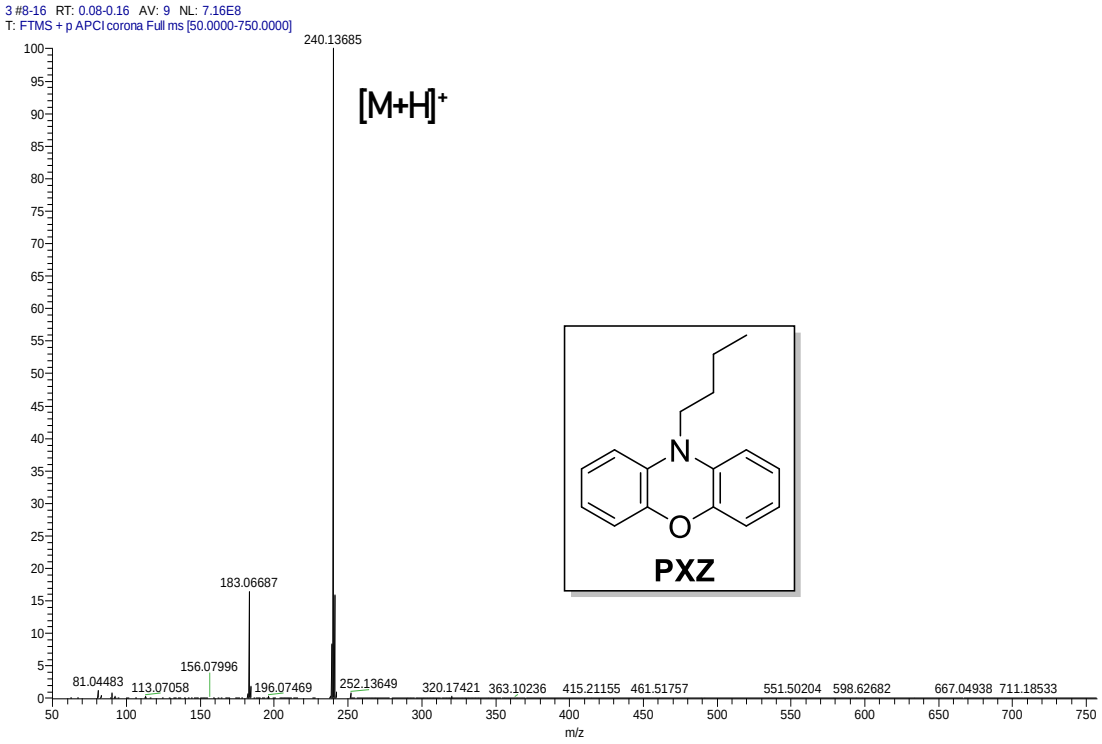

Fig. S2 APCI high resolution mass spectrum of **PXZ**.

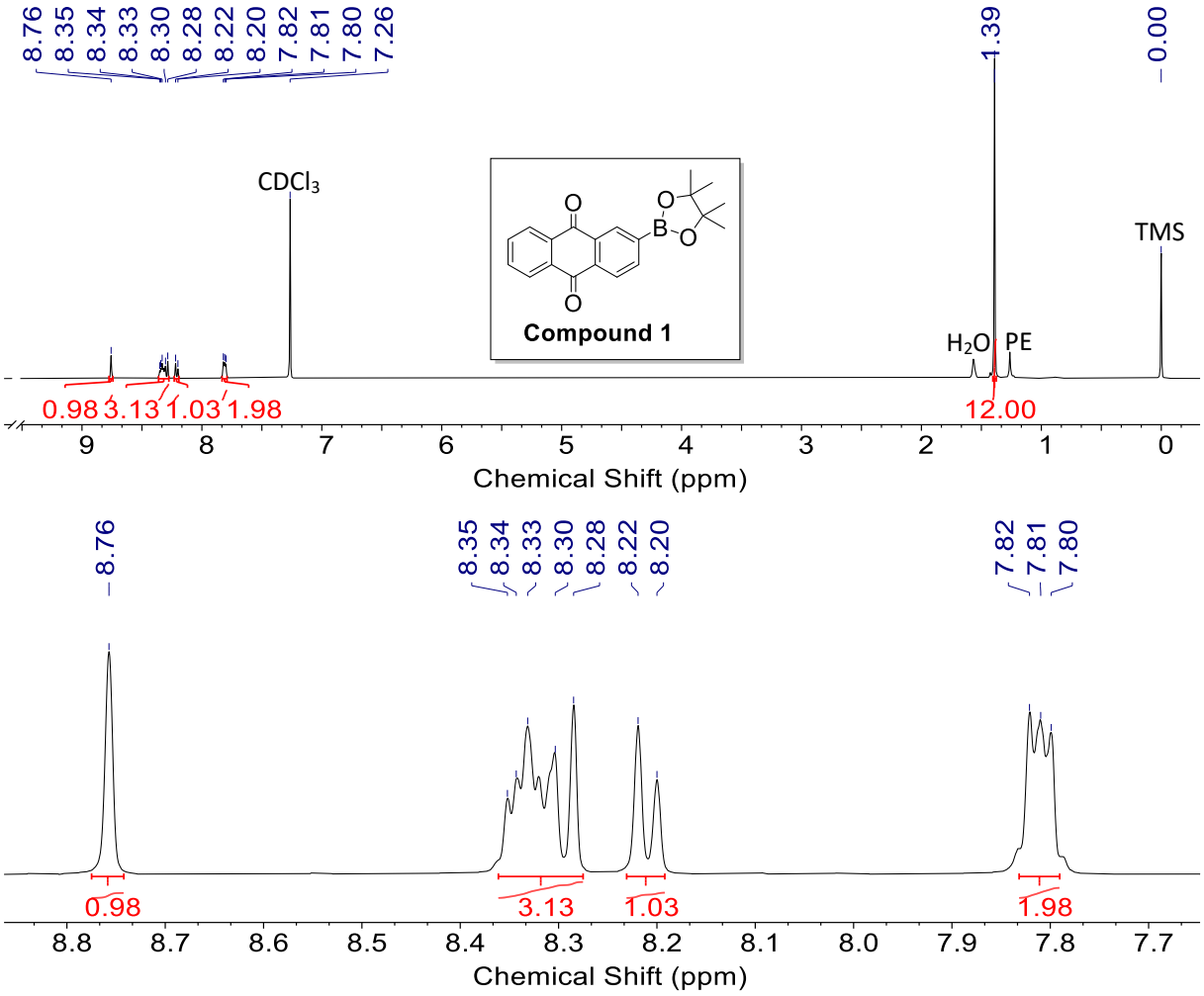

Fig. S3 ^{1}H NMR spectrum of Compound **1** (400 MHz, $CDCl_3$).

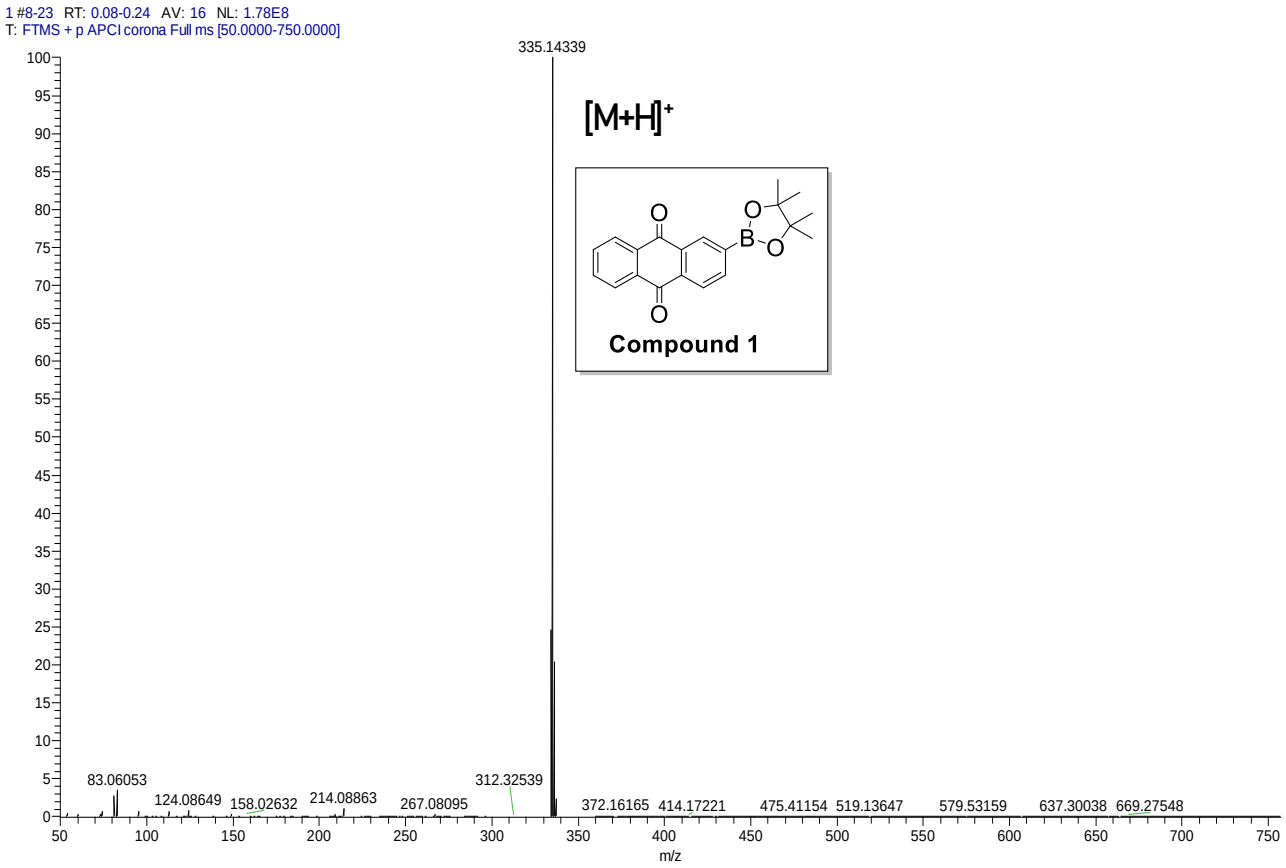

Fig. S4 APCI high resolution mass spectrum of Compound **1**.

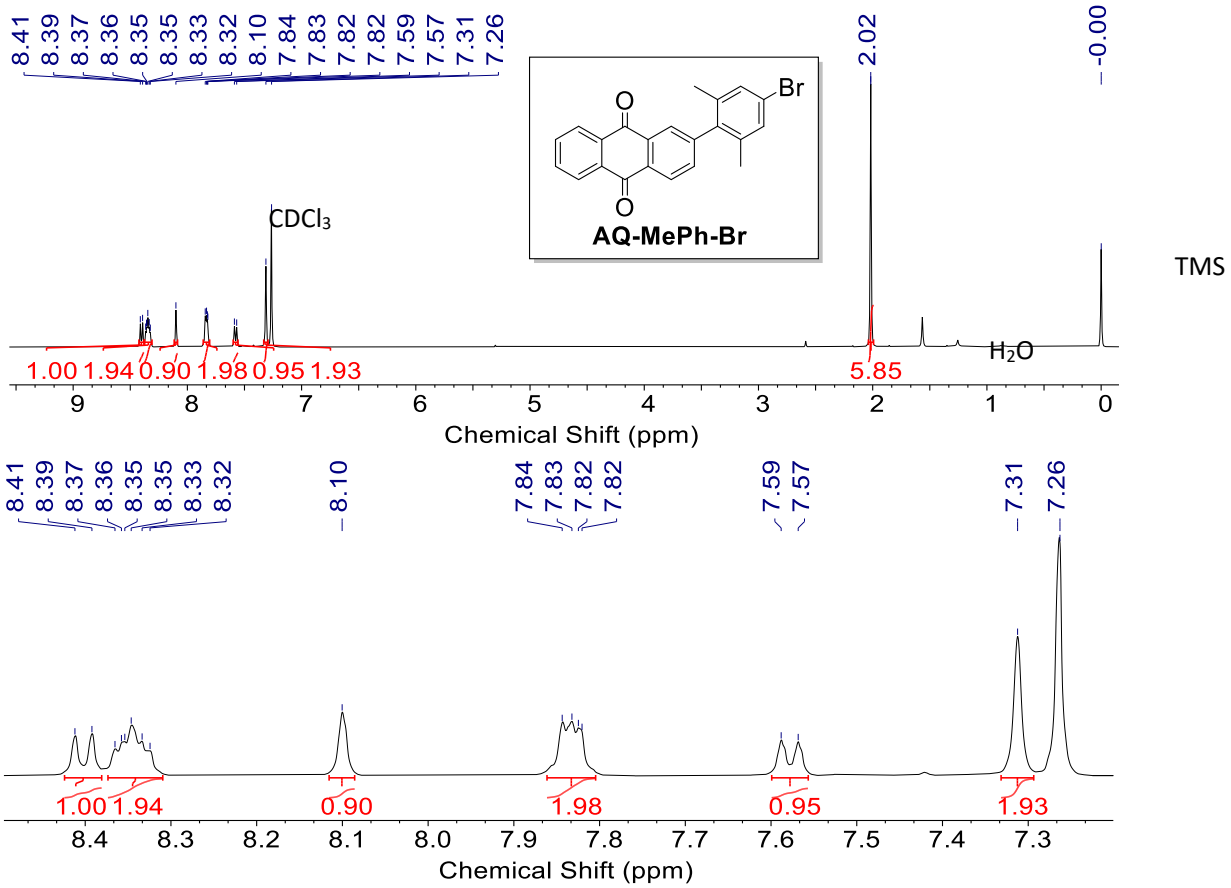

Fig. S5 ^{1}H NMR spectrum of **AQ-MePh-Br** (400 MHz, $CDCl_3$).

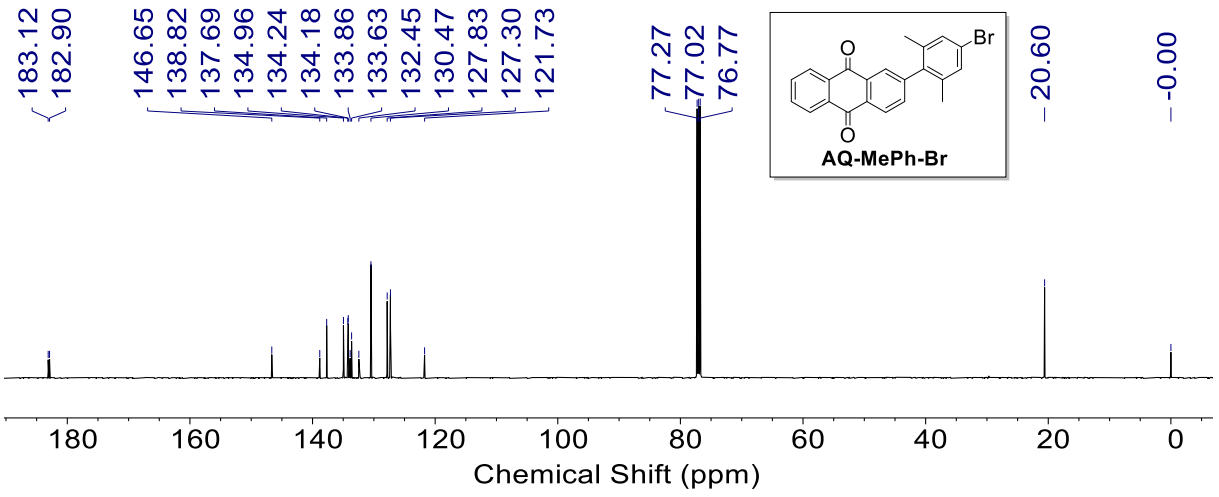

Fig. S6 ^{13}C NMR spectrum of **AQ-MePh-Br** (126 MHz, $CDCl_3$).

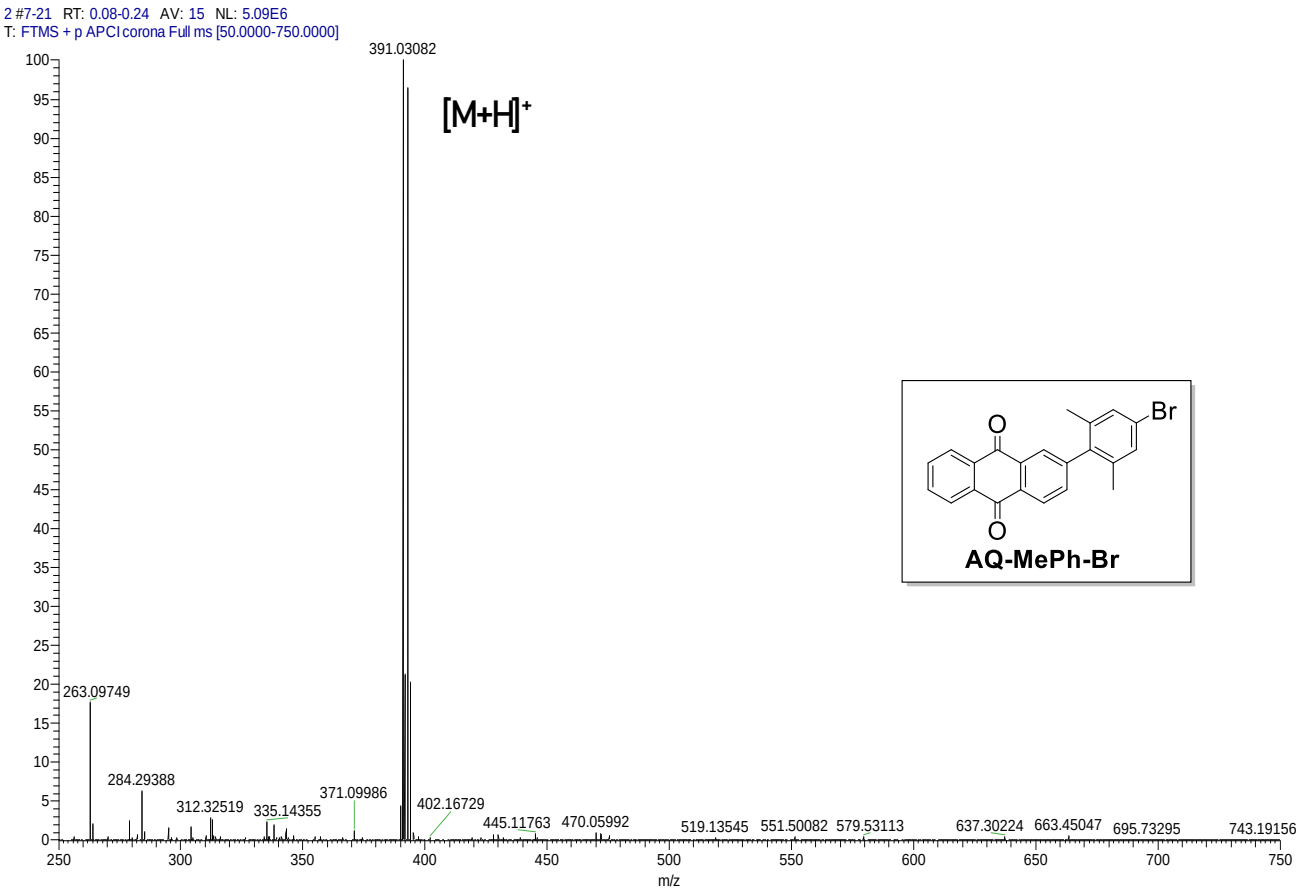

Fig. S7 APCI high resolution mass spectrum of **AQ-MePh-Br**.

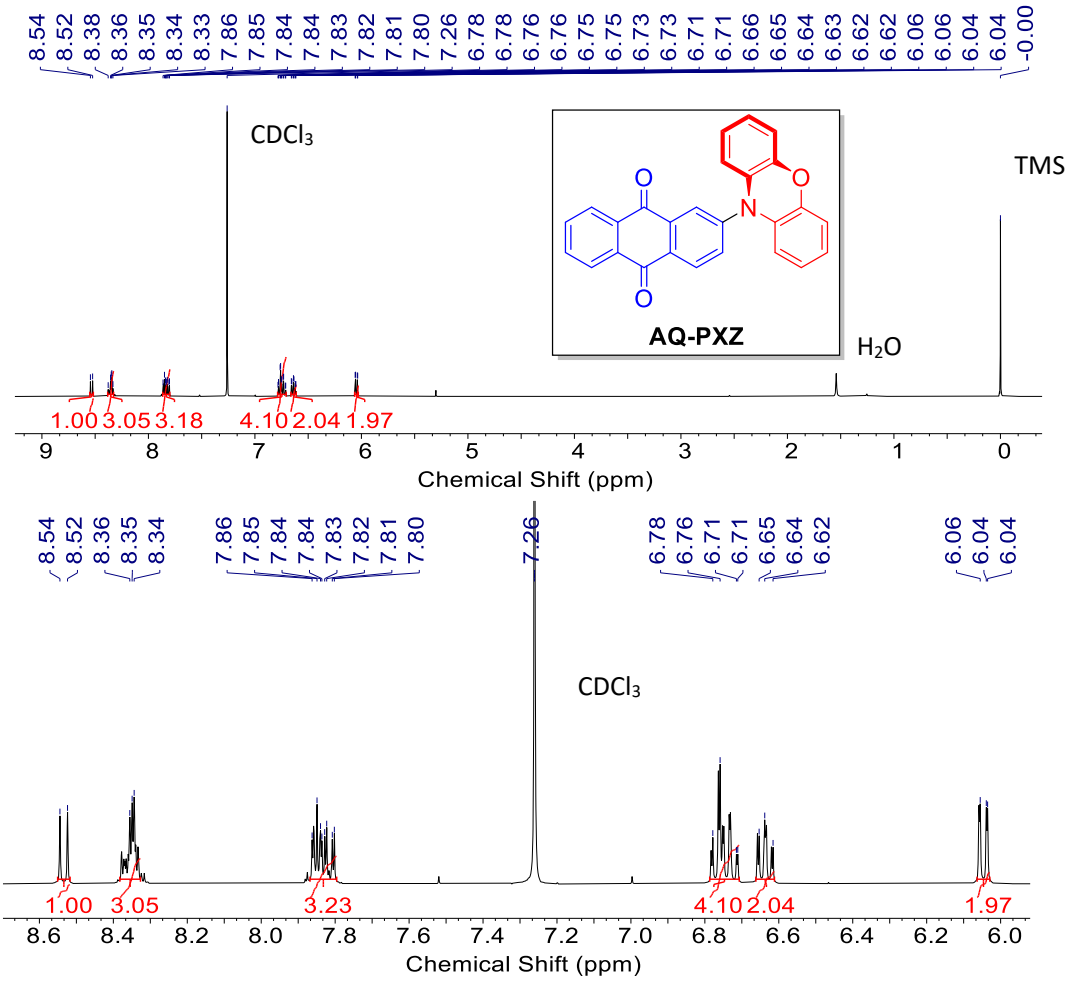

Fig. S8 ^{1}H NMR spectrum of **AQ-PXZ** (400 MHz, $CDCl_3$).

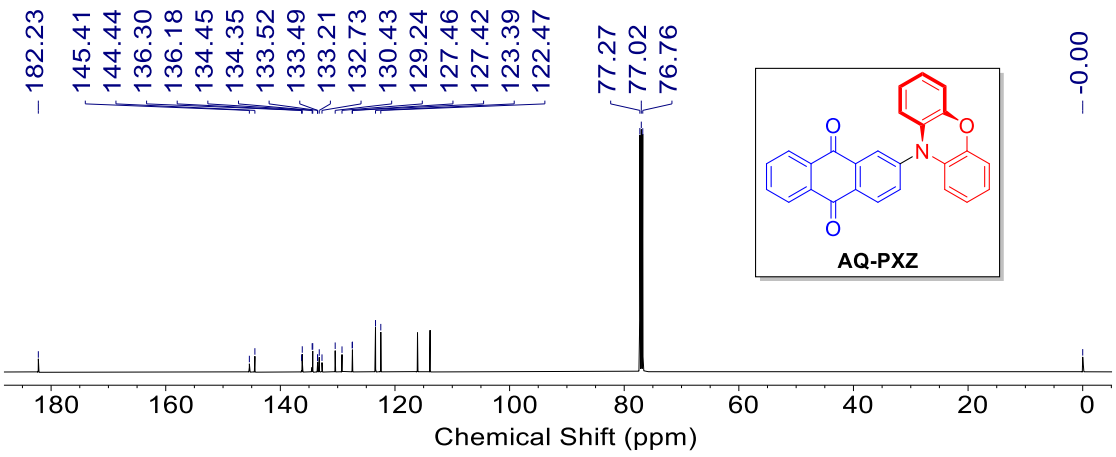

Fig. S9 ^{13}C NMR spectrum of **AQ-PXZ** (126 MHz, $CDCl_3$).

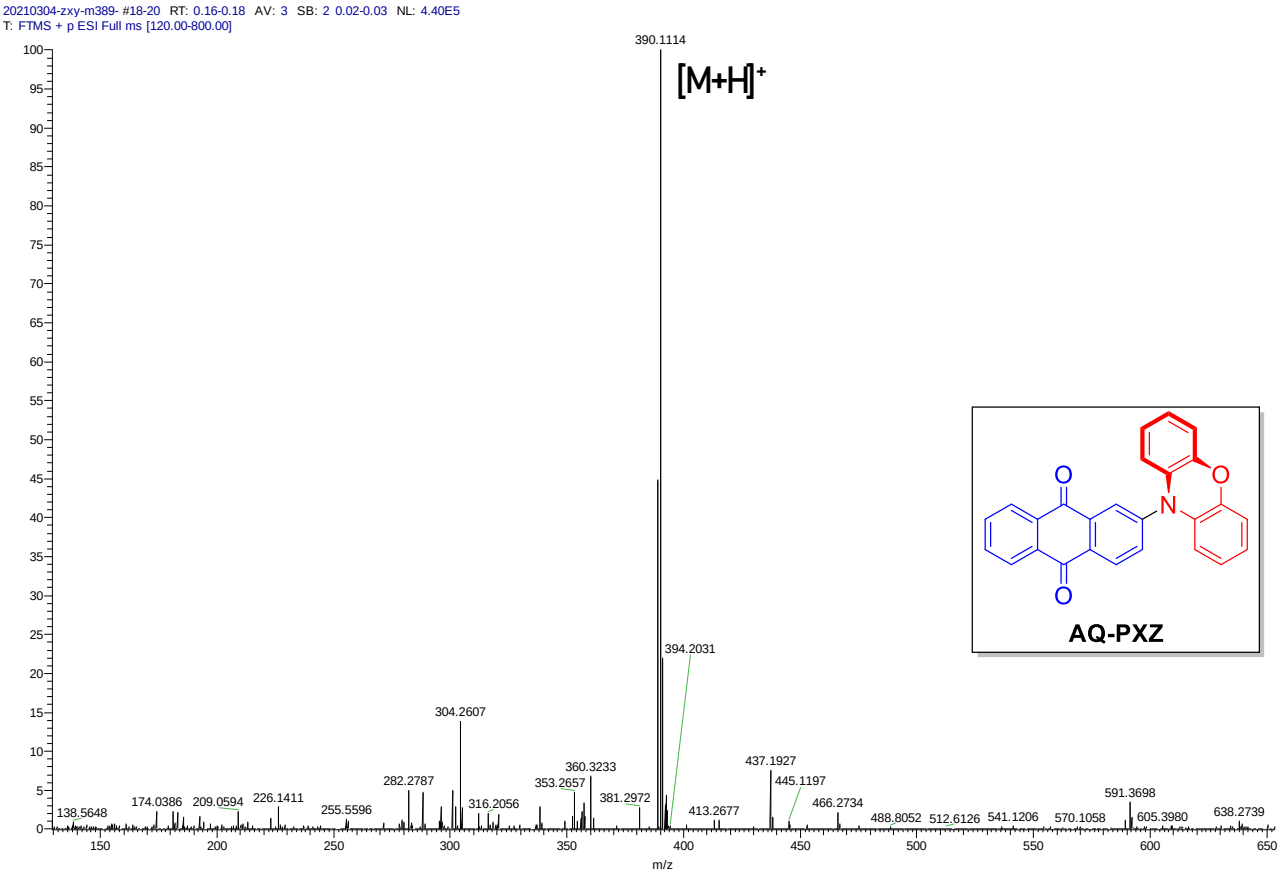

Fig. S10 ESI high resolution mass spectrum of **AQ-PXZ**.

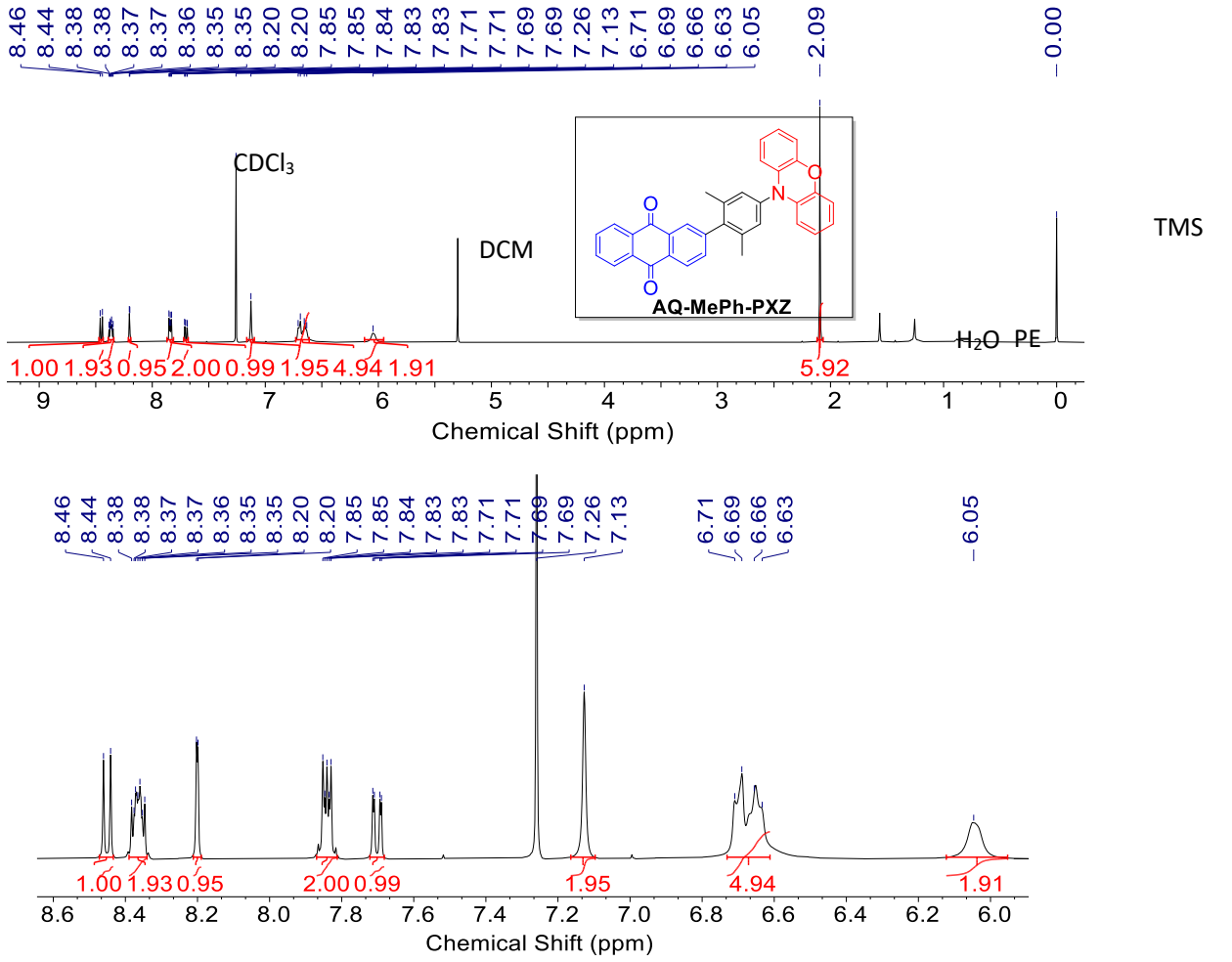

Fig. S11 ^{1}H NMR spectrum of **AQ-MePh-PXZ** (400 MHz, $CDCl_3$).

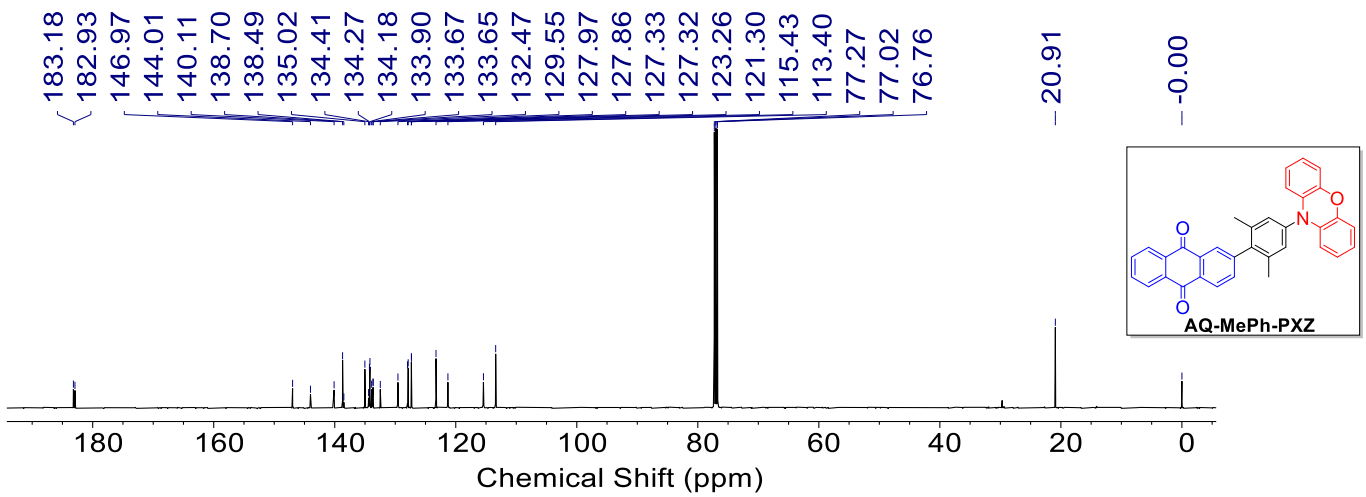

Fig. S12 ^{13}C NMR spectrum of **AQ-MePh-PXZ** (126 MHz, $CDCl_3$).

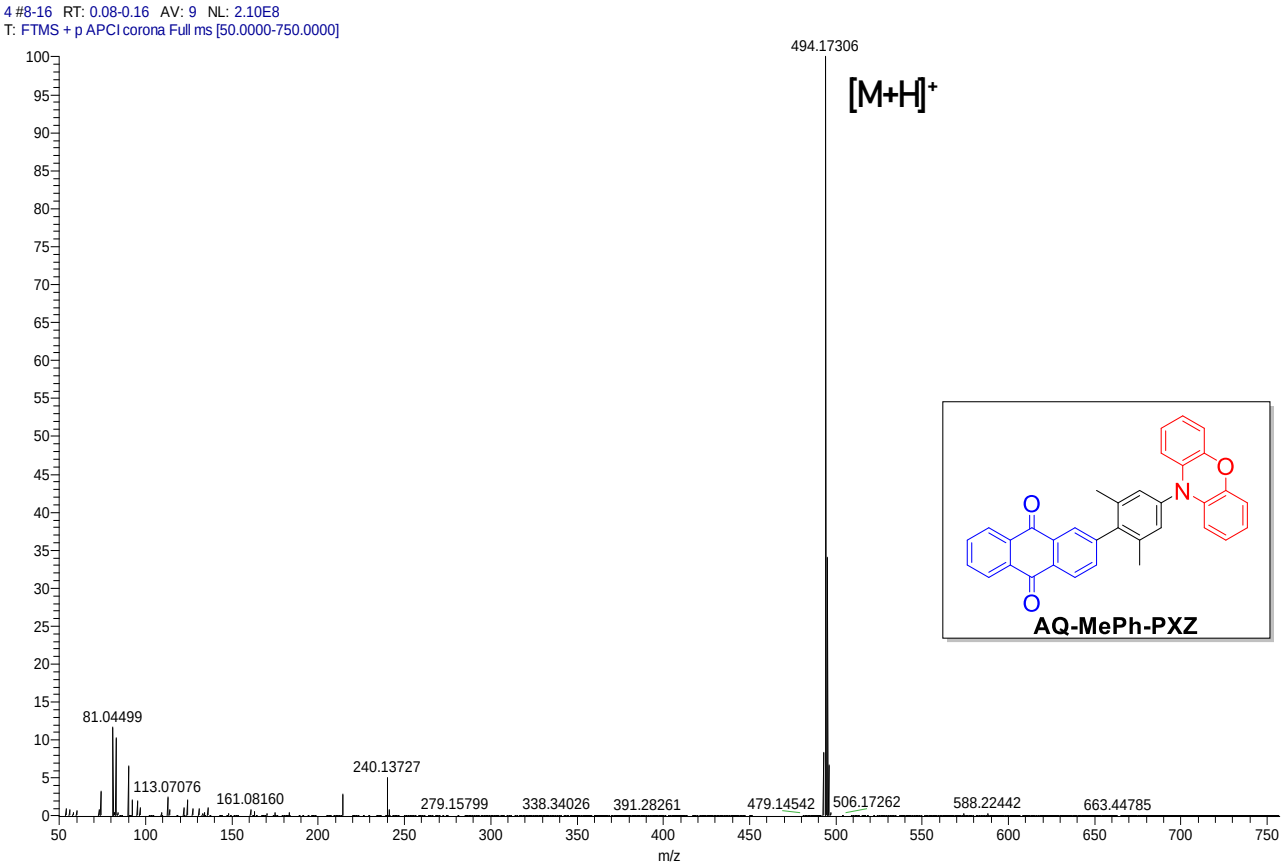

Fig. S13 APCI high resolution mass spectrum of **AQ-MePh-PXZ**.

4. Crystallographic Data

Table S1. Crystal Data for AQ-MePh-PXZ.

Compounds	**AQ-MePh-PXZ·CH_2Cl_2**
Sum formula	$C_{35}H_{25}Cl_2NO_3$
Formula weight	578.460
Temperature (K)	120
Wavelength (Å)	0.71073
Crystal system	Triclinic
Space group	P/–1
a (Å)	8.3400(8)
b (Å)	12.8996(14)
c (Å)	14.2181(15)
α (deg)	73.215(3)
β (deg)	73.872(3)
γ (deg)	85.302(3)
Volume ($Å^3$)	1406.8(3)
Z	2
Dx / g·cm^{-3}	1.366
crystal size (mm)	0.30×0.2×0.11
F (000)	600.0
μ / mm^{-1}	0.269
Theta range /deg	2.560– 24.942
R	0.0593
ωR_2	0.1650
T_{min} / T_{max}	0.708 / 0.745

5. Steady State UV-Vis Absorption Spectra

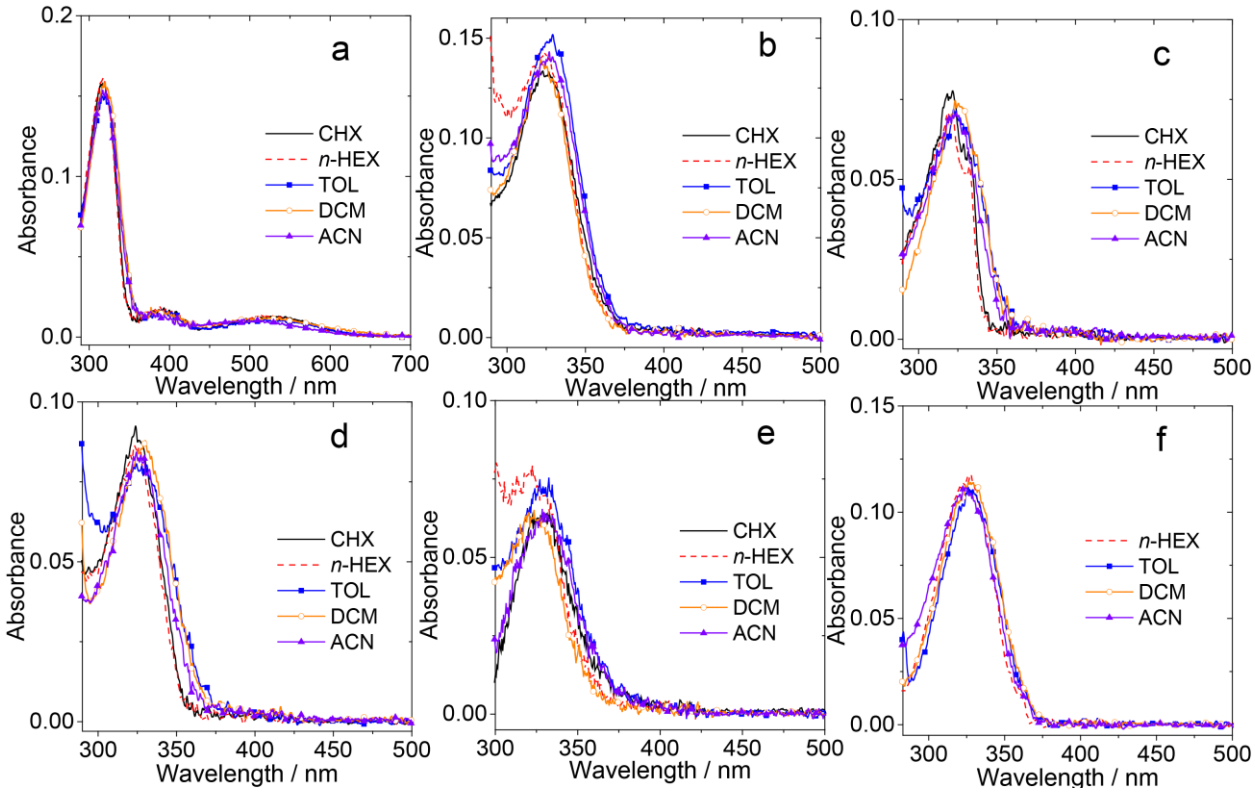

Fig. S14 UV−vis absorption spectra of (a) **AQ-PXZ**, (b) **AQ-MePh-PXZ**, (c) **AQ**, (d) **2-BrAQ**, (e) **AQ-MePh-Br** and (f) **PXZ** in different solvents. c = 1.0 × 10^{-5} M, 20 °C.

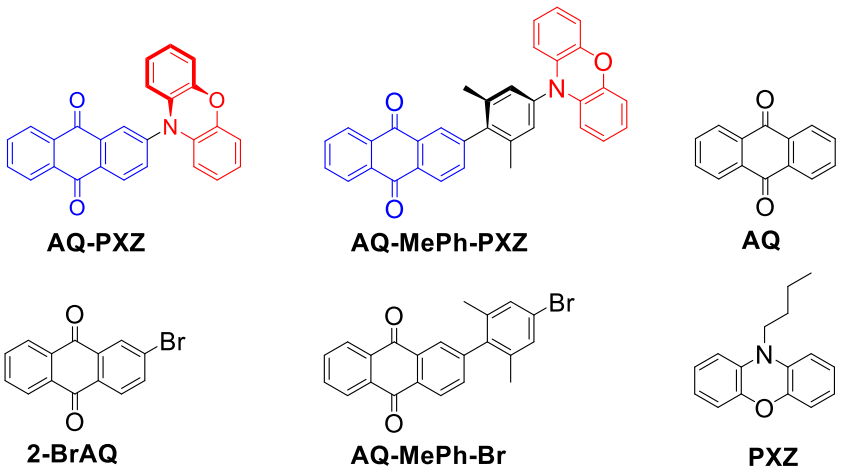

6. Fluorescence Spectra and Fluorescence Lifetime

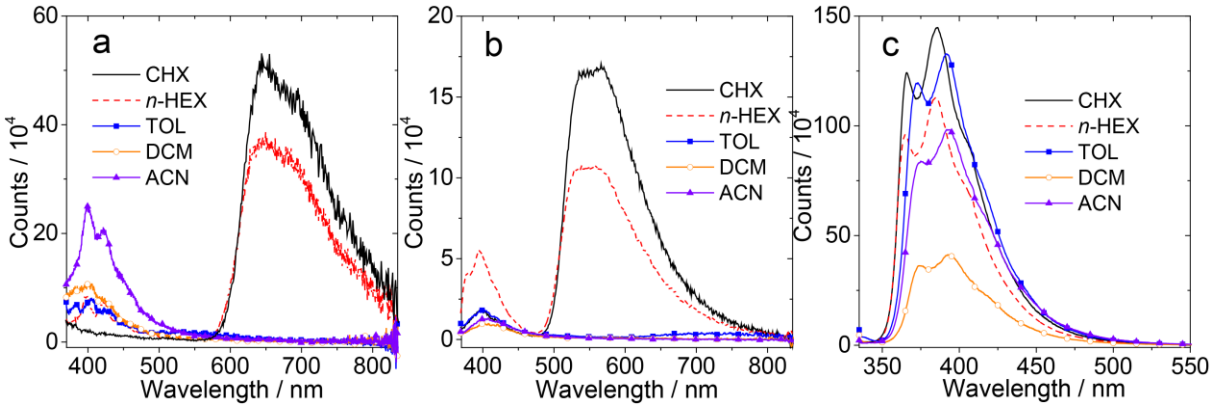

Fig. S15 Fluorescence emission spectra of (a) **AQ-PXZ**, (b) **AQ-MePh-PXZ** and (c) **PXZ** in different solvents. Optically matched solutions were used (λ_{ex} = 325 nm, A = 0.037), 20 °C.

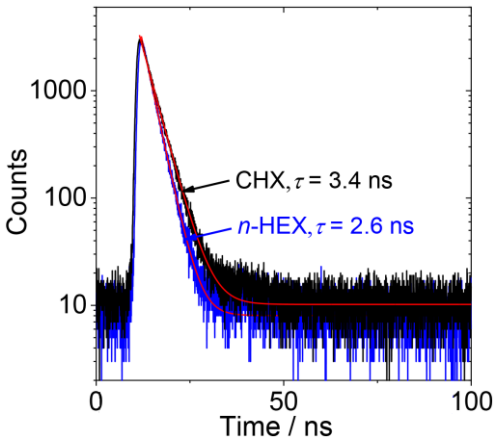

Fig. S16 Emission decay traces of **PXZ** monitor at 380 nm in different solvent, c = 1.0 × 10^{-5} M, λ_{ex} = 340 nm, 20 °C.

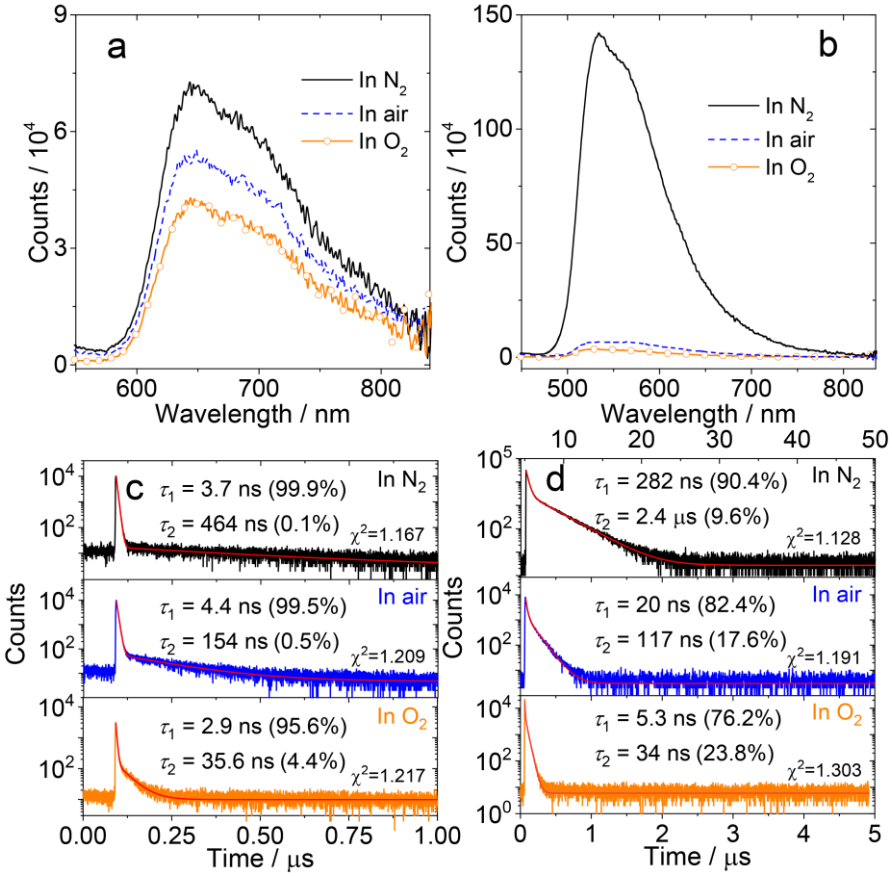

Fig. S17 Fluorescence emission spectra of (a) **AQ-PXZ** and (b) **AQ-MePh-PXZ** in different atmosphere. Optically matched solutions were used (λ_{ex} = 325 nm, A = 0.037). Decay traces in different atmosphere of (c) **AQ-PXZ** at 640 nm, c = 5.0 × 10^{-5} M and (d) **AQ-MePh-PXZ** at 550 nm, c = 3.0 × 10^{-5} M. λ_{ex} = 340 nm, 20 °C. The Reduced Chi-Square (χ^2) were presented to illustrate the quality of the fitting.

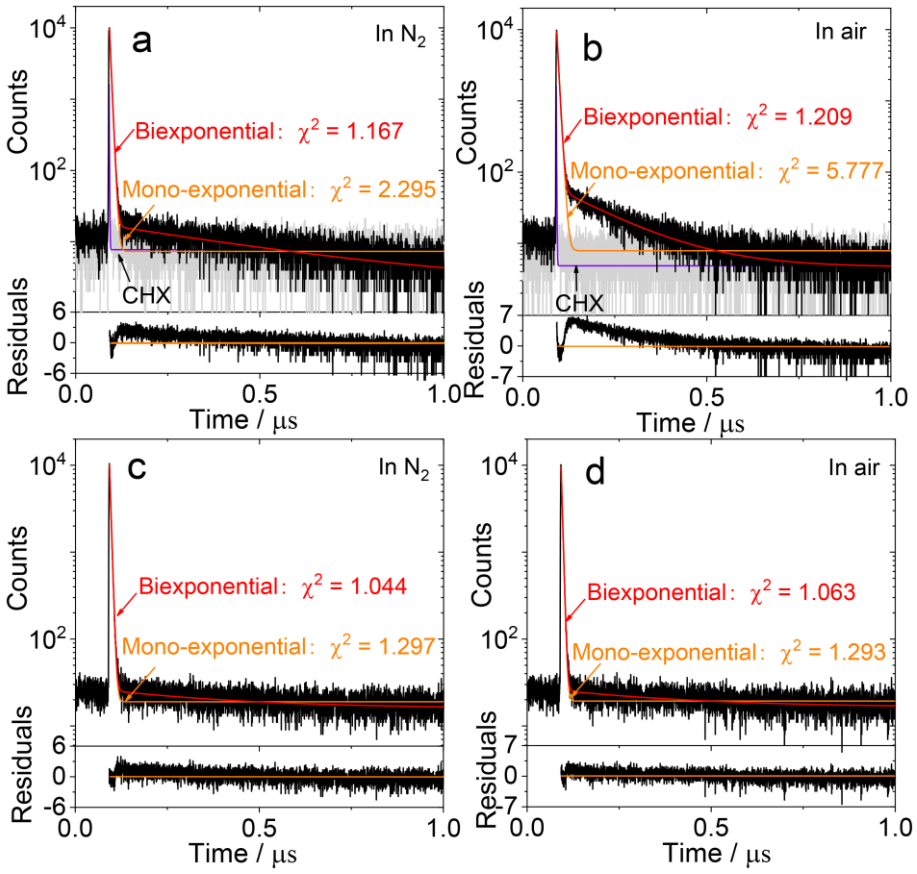

Fig. S18 Comparison of mono- and biexponential fitting the decay trace of **AQ-PXZ** (a) in N_2, (b) in air and **BDP-AN** (c) in N_2, (d) in air, c = 3.0 × 10^{-5} M. λ_{ex} = 340 nm, 20 °C. **BDP-AN** was act as a reference compound, which is a free-TADF compound.[6] For **AQ-PXZ**, the biexponential fitting is more reasonable due to its two emission components. The Reduced Chi-Square (χ^2) were presented to illustrate the goodness of fit.

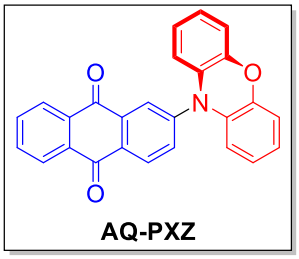

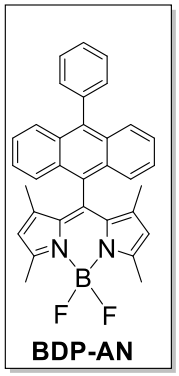

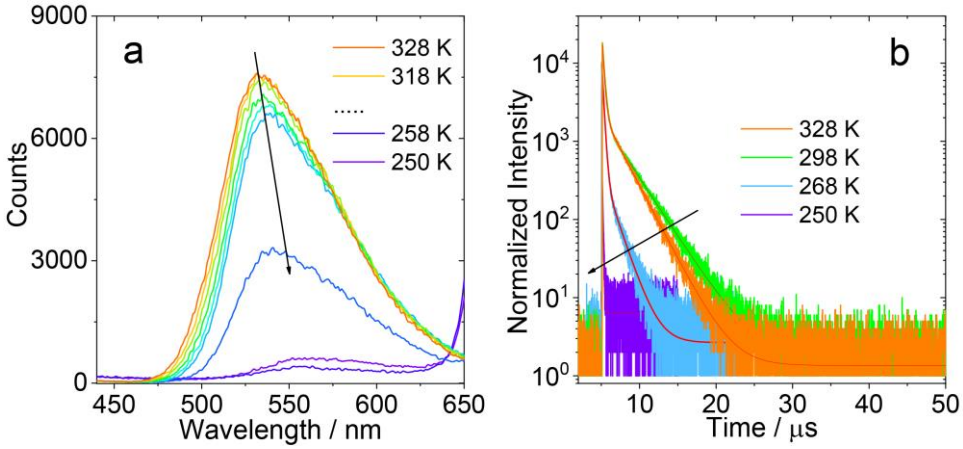

Fig. S19 (a) Temperature-dependent fluorescence emission spectra of **AQ-MePh-PXZ** in deaerated CHX, c = 3.0 × 10^{-5} M. (b) Temperature-dependent emission decay traces of **AQ-MePh-PXZ** in deaerated CHX, λ_{ex} = 340 nm.

Table S2. Temperature Dependent Emission Decay Traces Data of AQ-MePh-PXZ in Solution [a]

T / K	τ_1[b] / ns	Ratio[c] / %	τ_2[d] / ns	Ratio[e] / %
328	232	87.55	2301	12.45
298	271	89.96	2891	10.04
268	222	96.02	1468	3.98
250	2.69	91.33	_[f]	_[f]
	84.7	8.67		

[a] In deaerated CHX, c = 3.0 × 10^{-5} M, λ_{ex} = 340 nm. [b] Lifetime of the prompt fluorescence. [c] Ratio of the prompt fluorescence. [d] Lifetime of the delayed fluorescence. [e] Ratio of the delayed fluorescence. [f] Not observed.

Scheme S2. Putative Mechanism for Rationalization of the Temperature-Dependent TADF Property and the rISC Mechanism for AQ-MePh-PXZ[a]

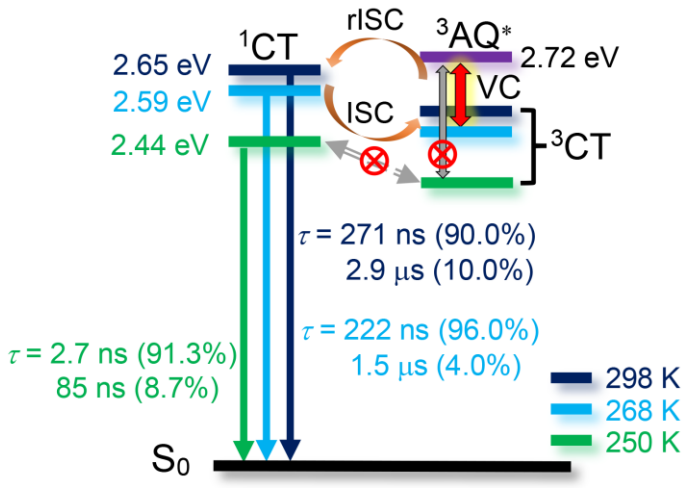

[a] VC: vibronic coupling. The energy levels of the ^{1}CT states are approximated from the onset of CT emission at the corresponding temperature. The energy level of ^{3}AQ state is obtained from reported result.[5] The energy levels of the ^{3}CT states are estimated similar to ^{1}CT states.

7. Electrochemical Characterization

The Gibbs free energy change (ΔG_{CS}) of the electron-transfer process was calculated using the Rehm-Weller equation (eq. S1–S3):[7,8]

$$\Delta G_{CS} = e[E_{OX} - E_{RED}] - E_{00} + \Delta G_S \quad \text{(eq. S1)}$$

$$\Delta G_S = -\frac{e^2}{4\pi\varepsilon_S\varepsilon_0 R_c} - \frac{e^2}{8\pi\varepsilon_0}\left(\frac{1}{R_D} + \frac{1}{R_A}\right)\left(\frac{1}{\varepsilon_{REF}} - \frac{1}{\varepsilon_S}\right) \quad \text{(eq. S2)}$$

$$E_{CS} = e\left[E_{OX} - E_{RED}\right] + \Delta G_S \quad \text{(eq. S3)}$$

in which ΔG_S is the static Coulombic energy, which is described by eq. S2. In eq. S1–S3, e is the electronic charge, E_{OX} is the half-wave potential for one-electron oxidation of the electron-donor unit (for irreversible oxidation, the anodic peak potential was used instead of the half-wave potential), and E_{RED} is the half-wave potential for one-electron reduction of the electron-acceptor unit, E_{00} is the energy level approximated with an average value between absorption and emission of **AQ** in CHX solution, ε_S is the static dielectric constant of the solvent, R_C is the center-to-center separation distance between electron donor and acceptor, determined by DFT optimization of the geometry, R_C (**AQ-PXZ**) = 6.8 Å, R_C (**AQ-MePh-PXZ**) = 11 Å. R_D is the radius of the electron donor, R_A is the radius of the electron acceptor, ε_{REF} is the static dielectric constant of the solvent used for the electrochemical studies, ε_0 is permittivity of free space. The solvents used in the calculation of free energy of the electron transfer is TOL (ε_S = 2.38), DCM (ε_S = 8.93) and ACN (ε_S = 37.5).

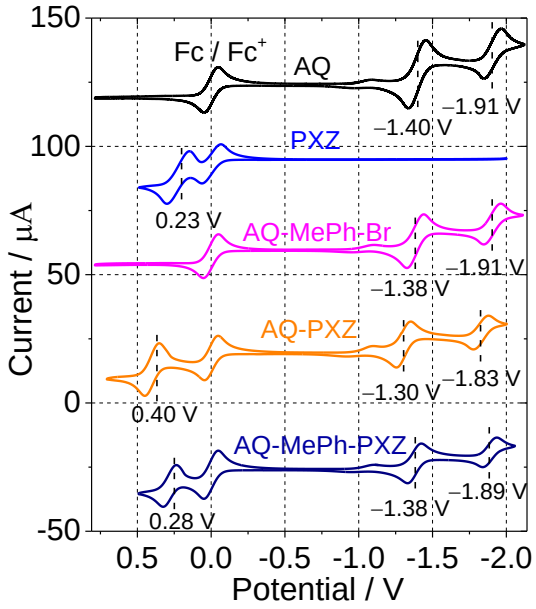

Fig. S20 Cyclic voltammograms of compounds in deaerated DCM containing 0.10 M tetrabutylammonium hexafluorophosphate ($Bu_4N[PF_6]$) as the supporting electrolyte and $Ag/AgNO_3$ as the reference electrode. Scan rate: 100 mV/s. Ferrocenium/ferrocene (Fc^+/Fc) redox couple was used as the internal reference, c = 1.0 × 10^{-3} M, 20 °C. The oxidation and reduction potential of compounds were presented.

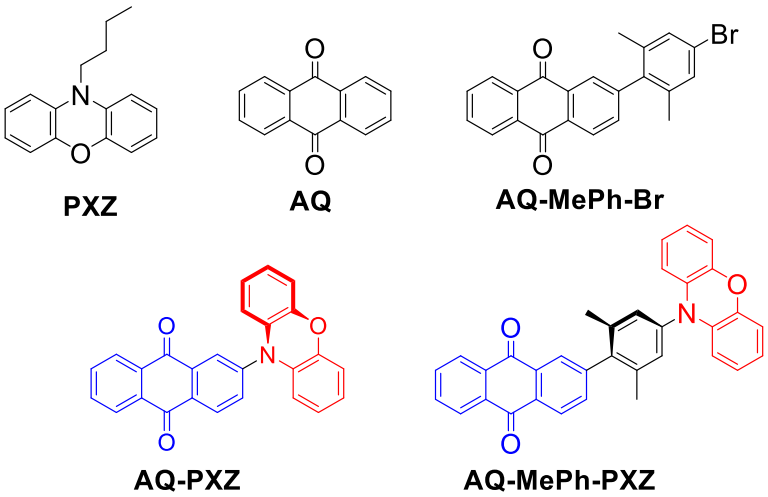

Table S3. Electrochemical Redox Potentials of the Compounds[a]

	E(ox) / V	*E*(red) / V	
PXZ	+0.23	–[b]	–[b]
AQ	–[b]	–1.40	–1.91
AQ-MePh-Br	–[b]	–1.38	–1.91
AQ-PXZ	+ 0.40	–1.30	–1.83
AQ-MePh-PXZ	+0.28	–1.38	–1.89

[a] Cyclic voltammetry measurements in N_2-saturated DCM containing a 0.10 M $BuN_4[PF_6]$ supporting electrolyte. Redox potentials of the compounds were determined with ferrocenium/ferrocene (Fc^+/Fc) redox couple as the internal standard (set as 0 V in the cyclic voltammograms). The counter electrode is the Pt electrode, the working electrode is the glassy carbon electrode, and the $Ag/AgNO_3$ couple is the reference electrode. [b] Not observed.

Table S4. Gibbs Free Energy of the Charge Separation (ΔG_{CS}) and Charge Separation Energy Levels (E_{CS}) of the Compounds in Different Solvents

	ΔG_{CS} (eV)				E_{CS} (eV)			
	n-HEX	TOL	DCM	ACN	*n*-HEX	TOL	DCM	ACN
AQ-PXZ[a]	–0.98	–1.17	–1.69	–1.84	2.18	1.99	1.47	1.32
AQ-MePh-PXZ[b]	–0.54	–0.83	–1.65	–1.87	2.62	2.33	1.51	1.29

[a] E_{00} = 3.16 eV. [b] E_{00} = 3.16 eV. The energy levels of E_{00} are approximated with an average value between absorption and emission of **AQ** in CHX.

8. UV-Vis Absorption Spectra of Radical Cation and Radical Anion

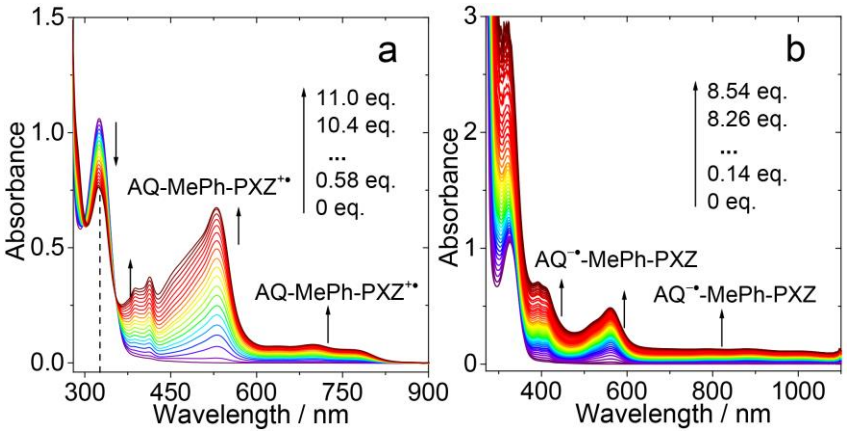

Fig. S21 Evolution of the UV-vis absorption spectra of **AQ-MePh-PXZ** (a) in the presence of increasing amount of nitrosonium hexafluorophosphate ($NO[PF_6]$) as oxidant in deaerated ACN. c = 8.5 x 10^{-5} M. (b) In the presence of increasing amount of cobaltocene ($CoCp_2$) as reductant in deaerated DMF, c = 1.0 x 10^{-4} M. 20 C.

9. Nanosecond Time-Resolved Transient Absorption Spectra

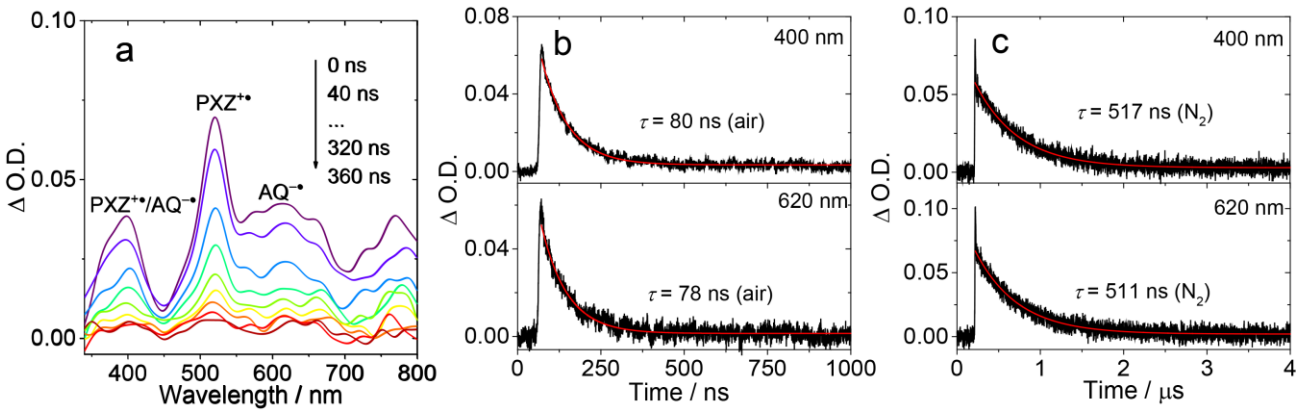

Fig. S22 (a) Nanosecond transient absorption spectra of **AQ-PXZ** in aerated CHX. Decay traces of **AQ-PXZ** at 400 nm and 620 nm (b) in aerated CHX and (c) in deaerated CHX, c = 1.0 × 10^{-4} M, 20 °C.

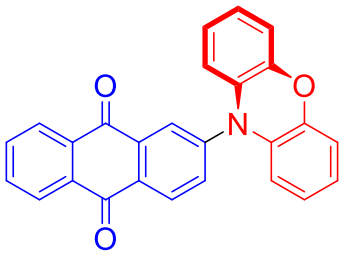

AQ-PXZ

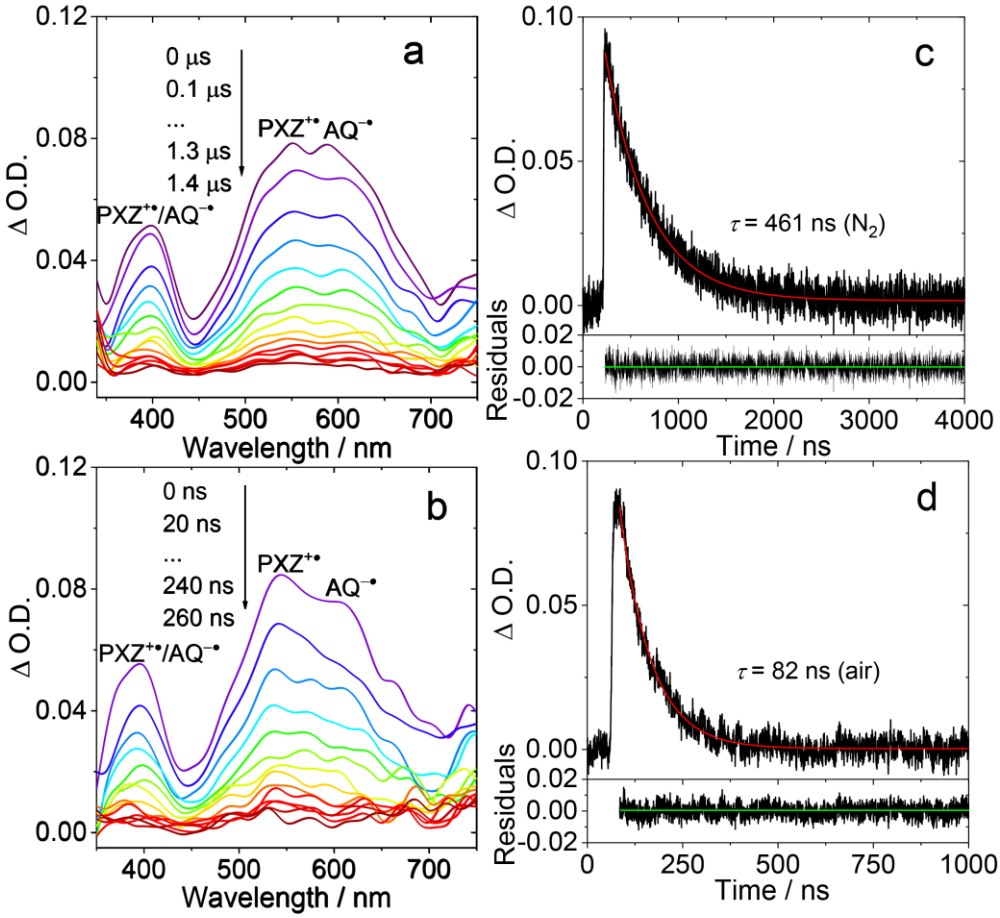

Fig. S23 Nanosecond transient absorption spectra of **AQ-PXZ** (a) in deaerated TOL and (b) in aerated TOL. Decay traces of **AQ-PXZ** at 550 nm (c) in deaerated TOL and (d) in aerated TOL, λ_{ex} = 355 nm, c = 1.0 × 10^{-4} M, 20 °C.

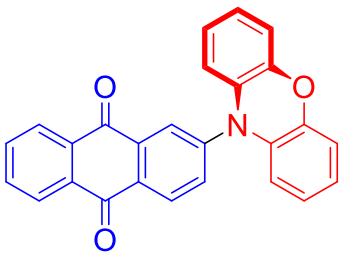

AQ-PXZ

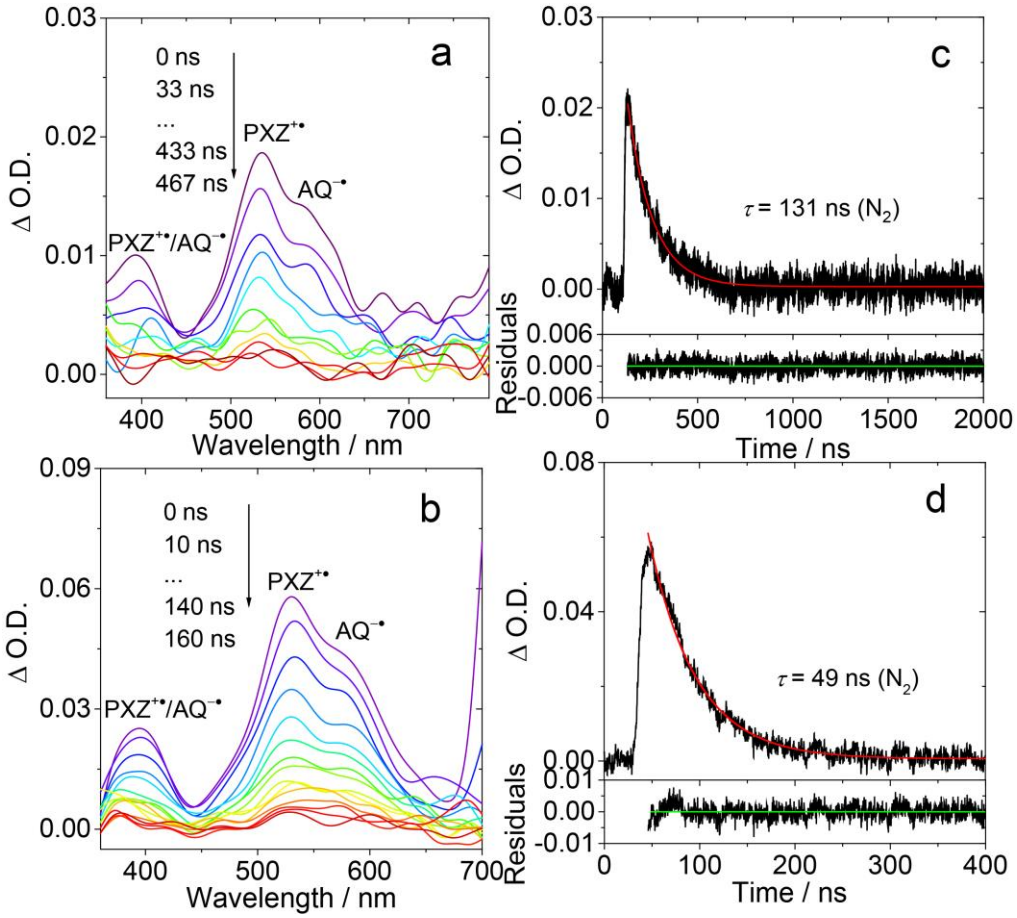

Fig. S24 Nanosecond transient absorption spectra of **AQ-PXZ** (a) in deaerated THF and (b) in deaerated ACN. Decay traces of **AQ-PXZ** at 530 nm (c) in deaerated THF and (d) in deaerated ACN, λ_{ex} = 355 nm, c = 1.0 × 10^{-4} M, 20 °C.

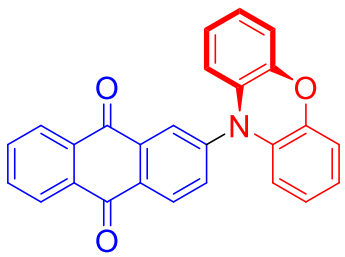

AQ-PXZ

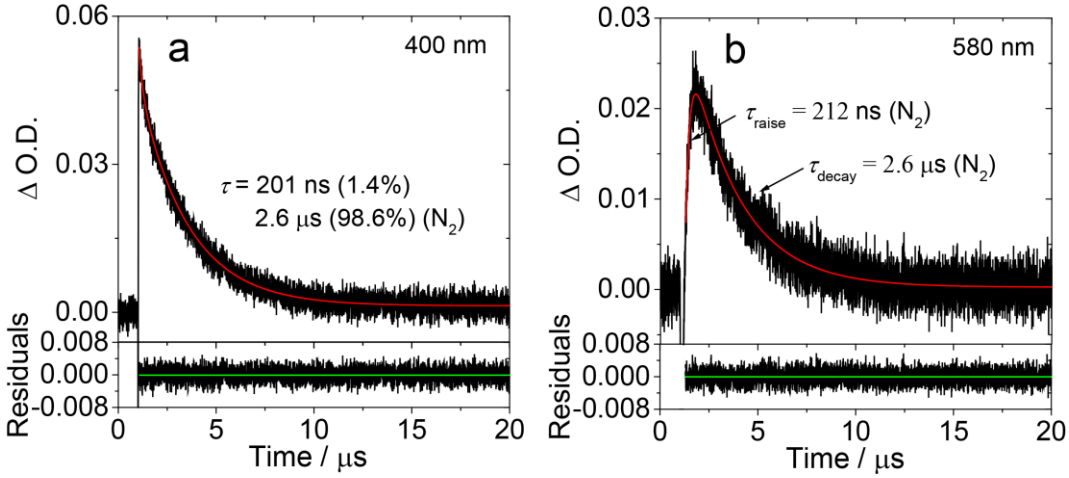

Fig. S25 Decay traces of **AQ-MePh-PXZ** (a) at 400 nm and (b) at 580 nm in deaerated CHX, λ_{ex} = 355 nm, c = 2.0 × 10^{-5} M, 20 °C.

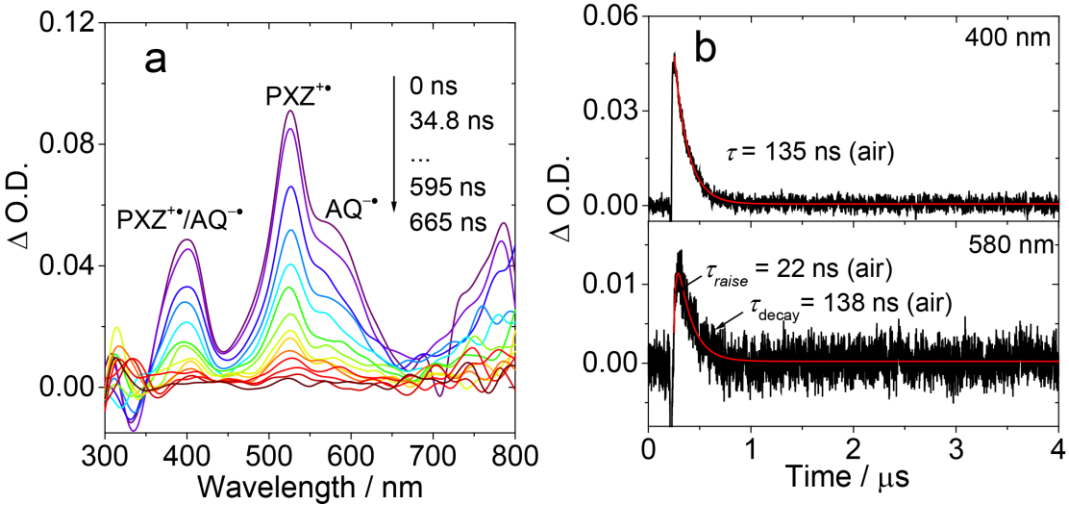

Fig. S26 (a) Nanosecond transient absorption spectra of **AQ-MePh-PXZ** in aerated CHX. (b) Decay traces of **AQ-MePh-PXZ** at 400 nm and 580 nm in aerated CHX, λ_{ex} = 355 nm, c = 2.0 × 10^{-5} M, 20 °C.

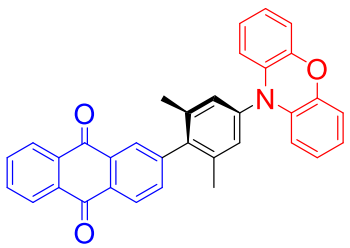

AQ-MePh-PXZ

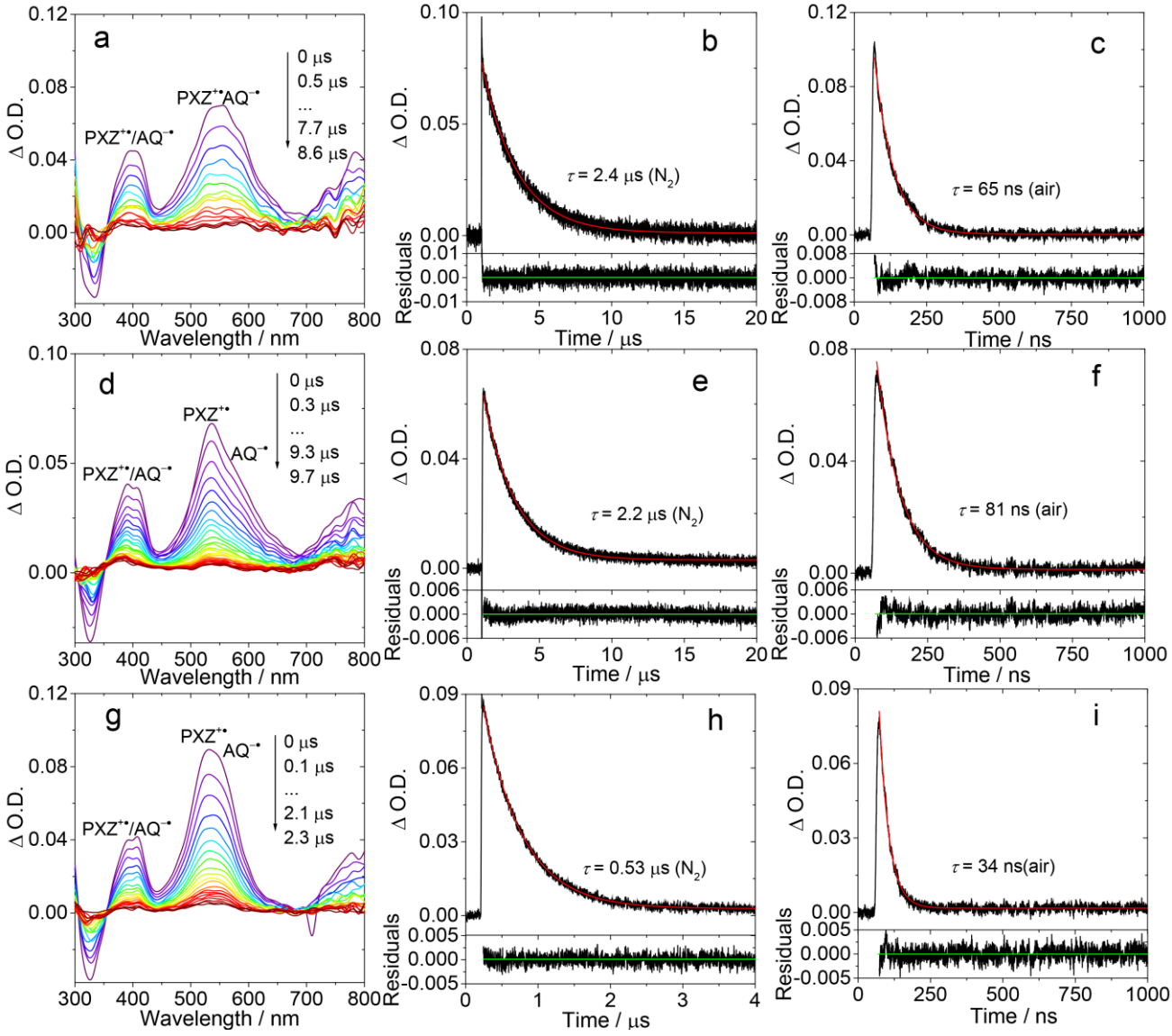

Fig. S27 Nanosecond transient absorption spectra of **AQ-MePh-PXZ** (a) in deaerated TOL, (d) in deaerated THF and (g) in deaerated ACN. Decay traces of **AQ-MePh-PXZ** (b), (c) at 560 nm in deaerated and aerated TOL; (e), (f) at 540 nm in deaerated and aerated THF; (h), (i) at 520 nm in deaerated and aerated ACN, λ_{ex} = 355 nm, c = 3.0 × 10^{-5} M, 20 °C.

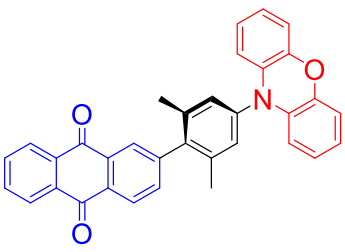

AQ-MePh-PXZ

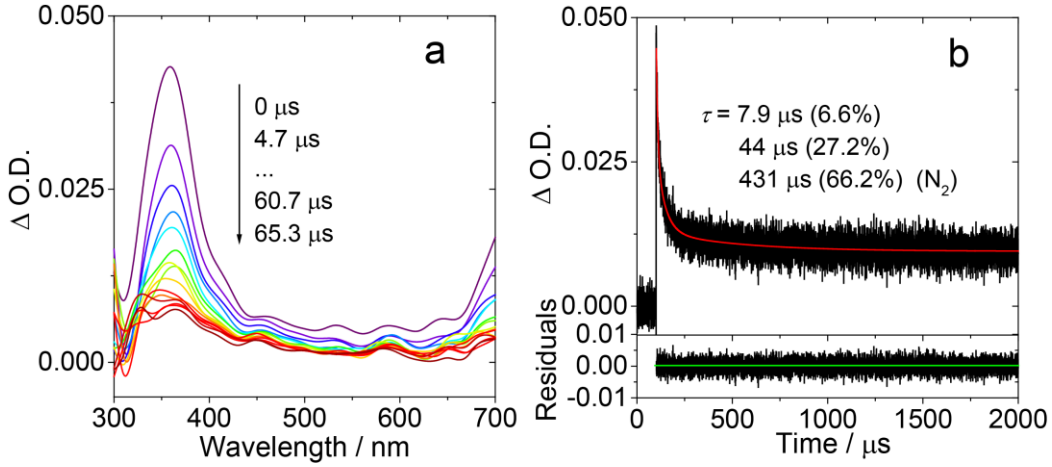

Fig. S28 (a) Nanosecond transient absorption spectra of **AQ** in deaerated CHX. (b) Decay traces of **AQ** at 370 nm in deaerated CHX, λ_{ex} = 355 nm, c = 1.0 × 10^{-4} M, 20 °C.

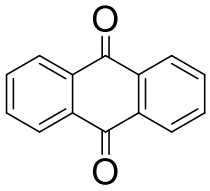

AQ

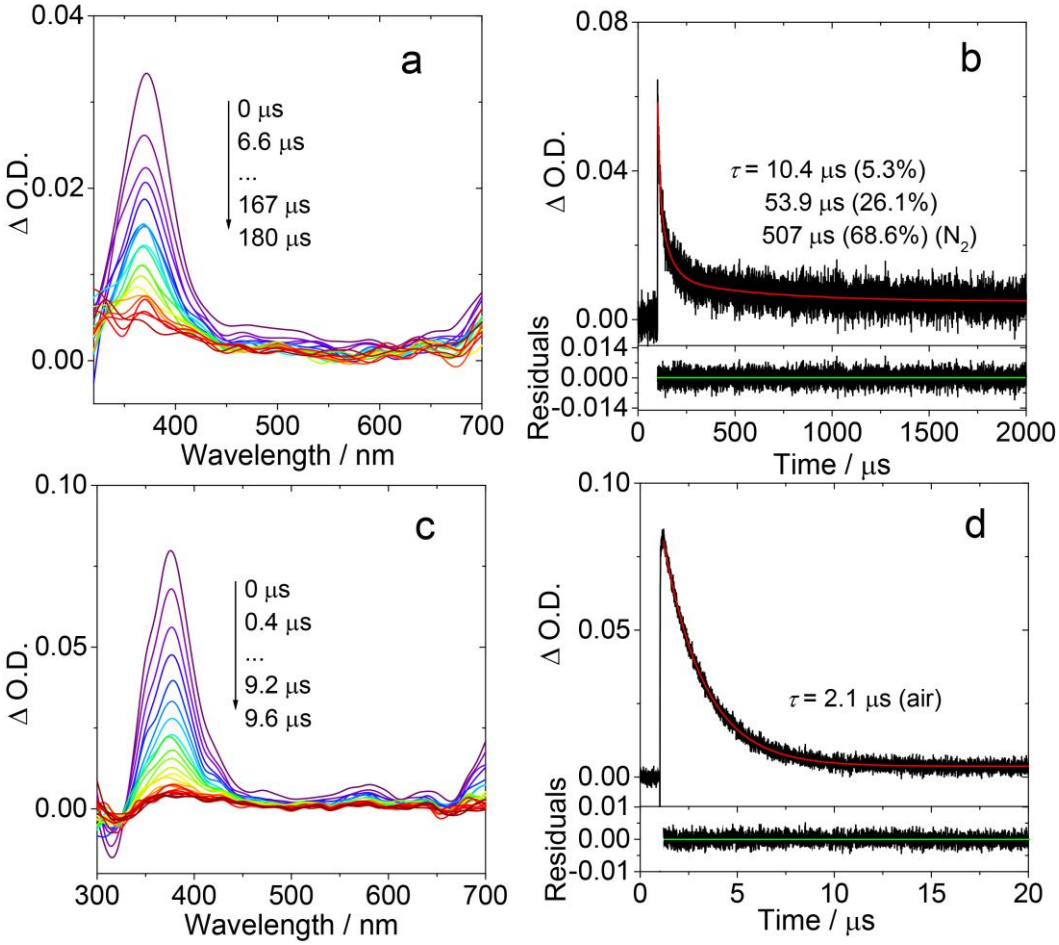

Fig. S29 Nanosecond transient absorption spectra of **AQ-MePh-Br** (a) in deaerated CHX and (c) in aerated CHX. Decay traces of **AQ-MePh-Br** at 370 nm (b) in deaerated and (d) in aerated CHX, λ_{ex} = 355 nm, c = 3.0 × 10^{-5} M, 20 °C.

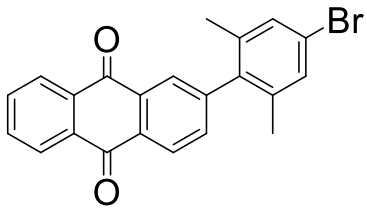

AQ-MePh-Br

10. DFT Calculations

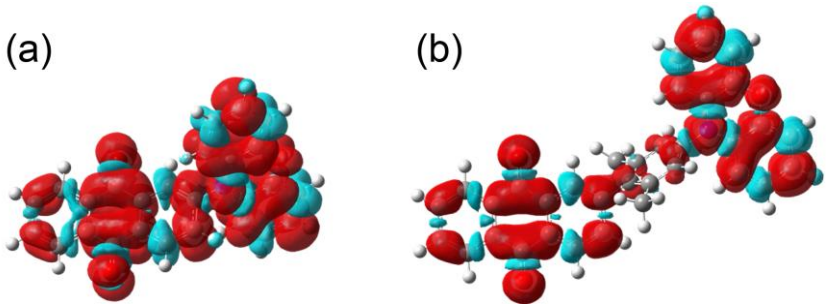

Fig. S30 Electron spin density surfaces of the triplet state of (a) **AQ-PXZ** and (b) **AQ-MePh-PXZ** in CHX (PCM model) at the optimized triplet state geometry, isovalue = 0.0004. Calculated at tuned CAM-B3LYP/6-31G (d) level with Gaussian 16.

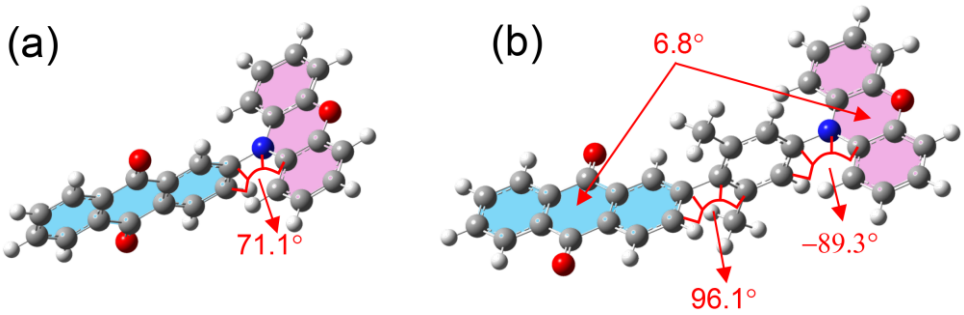

Fig. S31 Optimized ground state (S_0 state) geometries of **AQ-PXZ** and **AQ-MePh-PXZ** in CHX. Calculated at tuned CAM-B3LYP/6-31G (d) level with Gaussian 16. The dihedral angles between AQ and PXZ are presented.

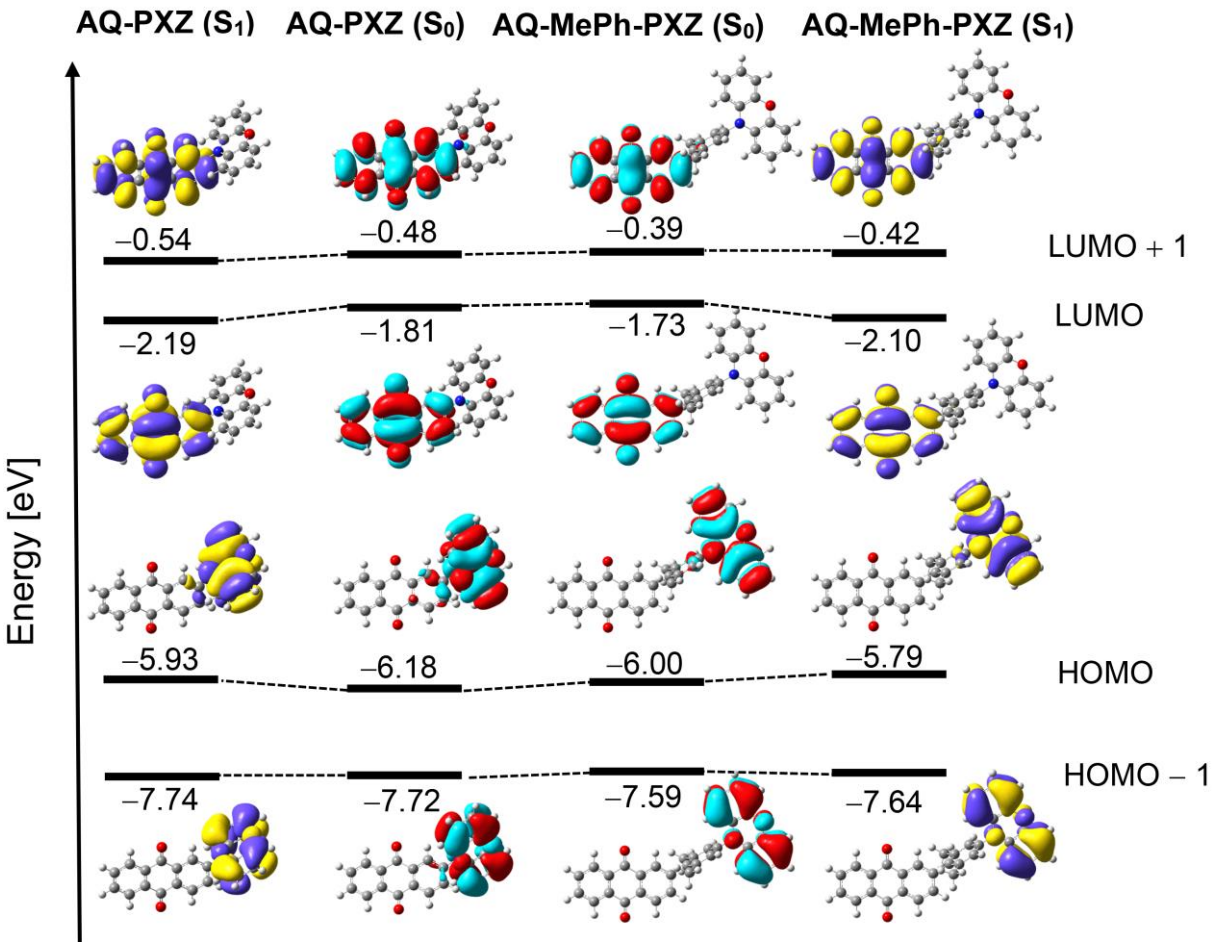

Fig S32. Selected frontier molecular orbitals of **AQ-PXZ** and **AQ-MePh-PXZ** at the ground state (S_0) and singlet excited state (S_1) calculated by DFT at tuned CAM-B3LYP/6-31G (d) in CHX, isovalue = 0.02. The energy levels of the orbits are presented (in eV).

Table S5. Electronic Excitation Energies (eV) and Corresponding Oscillator Strengths (*f*), Main Configurations, and CI Coefficients of the Low-Lying Electronic Excited States of AQ-PXZ in CHX (PCM model) were Presented. All Parameters were Calculated by TDDFT// tuned CAM-B3LYP/6-31G(d), Based on the DFT// tuned CAM-B3LYP/6-31G(d)-Optimized Ground State Geometries.

	Electronic transition [a]	Energy [b]	*f* [c]	CI [d]	Composition [e]	Assignment
Excitation	$S_0 \rightarrow T_1$	1.82 eV/681 nm	0.000	0.687	H → L	^{3}CT
	$S_0 \rightarrow T_2$	2.61 eV/476 nm	0.000	0.664	H–4 → L	^{3}AQ
	$S_0 \rightarrow T_3$	2.79 eV/444 nm	0.000	0.499	H → L+1	^{3}CT
	$S_0 \rightarrow T_4$	2.85 eV/435 nm	0.000	0.633	H–7 → L	^{3}AQ

[a] TDDFT// tuned CAM-B3LYP/6-31G(d), based on the DFT// tuned CAM-B3LYP/6-31G(d)-optimized ground state geometries in CHX (PCM model). [b] Only the selected low lying excited states are presented. [c] Oscillator strengths, no spin−orbital coupling effect was considered; thus, the *f* values are zero. [d] CI coefficients are in absolute values. [e] TDDFT// tuned- CAM-B3LYP/6-31G(d)-optimized excited state geometries.

Table S6. Electronic Excitation Energies (eV) and Corresponding Oscillator Strengths (*f*), Main Configurations, and CI Coefficients of the Low-Lying Electronic Excited States of AQ-MePh-PXZ in CHX (PCM model) were Presented. All Parameters were Calculated by TDDFT// tuned CAM-B3LYP/6-31G(d), Based on the DFT// tuned CAM-B3LYP/6-31G(d)-Optimized Ground State Geometries.

	Electronic transition [a]	Energy [b]	*f* [c]	CI [d]	Composition [e]	Assignment
Excitation	$S_0 \rightarrow T_1$	2.34 eV/530 nm	0.000	0.705	H → L	^{3}CT
	$S_0 \rightarrow T_2$	2.59 eV/478 nm	0.000	0.636	H–6 → L	^{3}CT
	$S_0 \rightarrow T_3$	2.84 eV/436 nm	0.000	0.650	H–10 → L	^{3}AQ
	$S_0 \rightarrow T_4$	2.86 eV/434 nm	0.000	0.584	H → L+6	^{3}CT

[a] TDDFT// tuned CAM-B3LYP/6-31G(d), based on the DFT// tuned CAM-B3LYP/6-31G(d)-optimized ground state geometries in CHX (PCM model). [b] Only the selected low lying excited states are presented. [c] Oscillator strengths, no spin−orbital coupling effect was considered; thus, the *f* values are zero. [d] CI coefficients are in absolute values. [e] TDDFT// tuned CAM-B3LYP/6-31G(d)-optimized excited state geometries.

11. Coordinates of the Optimized Geometries of the Compounds

AQ-PXZ

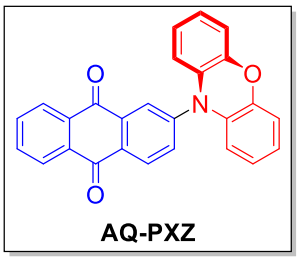

Calculation Type = FREQ

Calculation Method = RCAM-B3LYP

Basis Set = 6-31G(d)

Charge = 0

Spin = Singlet

Solvation = scrf=solvent=cyclohexane

E(RCAM-B3LYP) = -1279.583717 Hartree

RMS Gradient Norm = 0.002233 Hartree/Bohr

Imaginary Freq = 0

Dipole Moment = 2.393924 Debye

Point Group = C1

0 1

C	2.55465700	3.59283100	0.78788500
C	1.92641100	2.34938800	0.67912500
C	2.64693800	1.21222500	0.30213400
C	4.02452100	1.35453300	0.05988500
C	4.64891300	2.58806900	0.16504500
C	3.91467200	3.71941700	0.52842500
C	4.23339400	-0.95342000	-0.43404800
C	2.86027800	-1.15741600	-0.21277600
C	2.34388100	-2.43880000	-0.42757000
H	1.28400600	-2.61787800	-0.28610300
C	3.17555100	-3.48946400	-0.82402700
C	4.53466100	-3.27426400	-1.02343800
C	5.05953200	-1.99427200	-0.83004600
H	1.96640900	4.45750300	1.08027000
H	0.86699300	2.26428500	0.89245400
H	5.71452400	2.63994900	-0.03618800
H	4.40940300	4.68227300	0.60921900

H	2.74496400	-4.47432700	-0.97854300
H	5.18718800	-4.08545100	-1.33097000
H	6.11270000	-1.78029400	-0.98421000
N	2.05947300	-0.06612200	0.18664800
C	-6.80246600	0.03316600	-0.27641000
C	-5.84911000	-0.47870300	0.59919500
C	-4.48804100	-0.29338800	0.34075900
C	-4.08504500	0.41271300	-0.80849600
C	-5.04860900	0.92315700	-1.68305600
C	-6.40202000	0.73449100	-1.41822300
C	-3.48992600	-0.85301600	1.29287800
C	-2.64518400	0.62981800	-1.11579200
C	-1.64541800	0.07174100	-0.16005700
C	-2.04861800	-0.63687100	0.98569000
C	-1.08246800	-1.14850100	1.85725400
H	-1.41371800	-1.68675300	2.73928500
C	0.26877700	-0.95371800	1.59773800
C	0.67266300	-0.25314200	0.45159500
C	-0.28676600	0.25358100	-0.42532000
H	-7.85910800	-0.11304700	-0.07171200
H	-6.13532700	-1.02671200	1.49107800
H	-4.71339400	1.46370800	-2.56234700
H	-7.14760600	1.13304000	-2.10013000
H	1.02446300	-1.33965900	2.27526200
H	0.00789100	0.79299200	-1.31972900
O	-2.28975500	1.24487400	-2.11478500
O	-3.83801900	-1.47064700	2.29354400
O	4.82617800	0.28231000	-0.27554300

AQ-MePh-PXZ

Calculation Type = FREQ

Calculation Method = RCAM-B3LYP

Basis Set = 6-31G(d)

Charge = 0

Spin = Singlet

Solvation = scrf=solvent=cyclohexane

E(RCAM-B3LYP) = -1589.087975 Hartree

RMS Gradient Norm = 0.002052 Hartree/Bohr

Imaginary Freq = 0

Dipole Moment = 3.312292 Debye

Point Group = C1

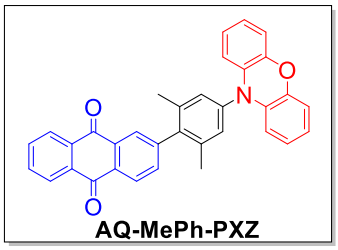

0 1

C	5.42036900	-3.38352600	-0.18862200
C	4.50702900	-2.32745400	-0.12127100
C	4.94822400	-1.00247200	-0.06071400
C	6.33465000	-0.76468300	-0.06957200
C	7.24105900	-1.81094600	-0.13724800
C	6.78765800	-3.13202400	-0.19712300
C	5.98130700	1.57794300	0.03988600
C	4.58670400	1.39544000	0.05116200
C	3.77412800	2.53147700	0.10490400
H	2.69651600	2.41029300	0.11433700
C	4.33525700	3.81106200	0.14674400
C	5.71579800	3.97491700	0.13465700
C	6.53878400	2.84616700	0.08037100
H	5.04797800	-4.40283500	-0.23432100
H	3.44163400	-2.52974900	-0.11515700
H	8.29994900	-1.57096100	-0.14135300
H	7.50306600	-3.94694600	-0.24943500
H	3.67866000	4.67523300	0.18859500
H	6.15884100	4.96553400	0.16678800

H	7.62125500	2.92987200	0.06925000
N	4.06530000	0.08975900	0.00928100
C	2.65008900	-0.12384000	0.01842400
C	1.97651600	-0.27603600	1.22907600
C	1.94474300	-0.17884500	-1.18253500
C	0.59479000	-0.48494300	1.25665100
H	2.53900100	-0.22854100	2.15765000
C	0.56233800	-0.38485000	-1.19052500
H	2.48302700	-0.05951700	-2.11898100
C	-0.11047900	-0.53874100	0.03796400
C	-2.47507200	0.31692400	-0.02317100
C	-3.85696100	0.11310500	-0.01225900
C	-1.58950000	-0.76208400	0.04870300
C	-4.76097400	1.29576700	-0.08980500
C	-4.37178800	-1.19282600	0.07112000
C	-2.11672200	-2.06185700	0.13179900
C	-6.22826500	1.04208400	-0.07513400
C	-5.83876600	-1.44714100	0.08486600
C	-3.49083200	-2.27532100	0.14246000
H	-1.43644400	-2.90779800	0.18612000
C	-7.10457200	2.12892100	-0.14580900
C	-6.74234700	-0.26570100	0.00828500
H	-3.90570400	-3.27623000	0.20519500
C	-8.48048500	1.91886600	-0.13365400
H	-6.68402500	3.12731500	-0.20953500
C	-8.12534200	-0.46805900	0.01992500
C	-8.99120500	0.61950600	-0.05069700
H	-9.15793400	2.76617000	-0.18874600
H	-8.49706100	-1.48554000	0.08482500
H	-10.06529200	0.45779400	-0.04133600
O	-4.31158600	2.43442700	-0.16304900
O	-6.28507500	-2.58729800	0.15681700
C	-0.18298600	-0.44216800	-2.50258800
H	-0.73692600	-1.38214400	-2.60991300
H	-0.91770100	0.36760200	-2.58442500
H	0.50820900	-0.35650700	-3.34596500
C	-0.11713900	-0.63984600	2.57935100
H	-0.90649200	0.11132500	2.70015300

H	-0.59974800	-1.62048800	2.66683200
H	0.58355000	-0.53321300	3.41241300
H	-2.10474100	1.33575400	-0.08683000
O	6.85881600	0.51191500	-0.00937400

12. Reference

(1) T. Lu Optdftw Program V1.0. http://sobereva.com/346.

(2) H. Noda, X. K. Chen, H. Nakanotani, T. Hosokai, M. Miyajima, N. Notsuka, Y. Kashima, J. L. Bredas and C. Adachi, *Nat. Mater.*, 2019, ***18***, 1084–1090.

(3) M. J. Frisch, G. W. Trucks, H. B. Schlegel, G. E. Scuseria, M. A. Robb, J. R. Cheeseman, G. Scalmani, V. Barone, G. A. Petersson, H. Nakatsuji, X. Li, M. Caricato, A. V. Marenich, J. Bloino, B. G. Janesko, R. Gomperts, B. Mennucci, H. P. Hratchian, J. V. Ortiz, A. F. Izmaylov, J. L. Sonnenberg, D. Williams-Young, F. Ding, F. Lipparini, F. Egidi, J. Goings, B. Peng, A. Petrone, T. Henderson, D. Ranasinghe, V. G. Zakrzewski, J. Gao, N. Rega, G. Zheng, W. Liang, M. Hada, M. Ehara, K. Toyota, R. Fukuda, J. Hasegawa, M. Ishida, T. Nakajima, Y. Honda, O. Kitao, H. Nakai, T. Vreven, K. Throssell, J. A. Montgomery, Jr., J. E. Peralta, F. Ogliaro, M. J. Bearpark, J. J. Heyd, E. N. Brothers, K. N. Kudin, V. N. Staroverov, T. A. Keith, R. Kobayashi, J. Normand, K. Raghavachari, A. P. Rendell, J. C. Burant, S. S. Iyengar, J. Tomasi, M. Cossi, J. M. Millam, M. Klene, C. Adamo, R. Cammi, J. W. Ochterski, R. L. Martin, K. Morokuma, O. Farkas, J. B. Foresman, and D. J. Fox, *Gaussian 16 Rev. B. 01*, Gaussian Inc.: Wallingford, CT, 2016.

(4) Y. Dong, A. A. Sukhanov, J. Zhao, A. Elmali, X. Li, B. Dick, A. Karatay and V. K. Voronkova, *J. Phys. Chem. C*, 2019, ***123***, 22793–22811.

(5) M. Montalti, A. Credi, L. Prodi and M. T. Gandolfi, *Handbook of Photochemistry*, 3rd ed.; CRC Press: Boca Raton, 2006.

(6) Z. Wang and J. Zhao, *Org. Lett.*, 2017, **19**, 4492–4495.

(7) R. Ziessel, B. D. Allen, D. B. Rewinska and A. Harriman, *Chem. –Eur. J.*, 2009, ***15***, 7382–7393.

(8) W.-J. Shi, M. E. El-Khouly, K. Ohkubo, S. Fukuzumi and D. K. P. Ng, *Chem. –Eur. J.*, 2013, ***19***, 11332–11341.